

Numerical solution of the dynamical mean field theory of infinite-dimensional equilibrium liquids

Alessandro Manacorda,¹ Grégory Schehr,² and Francesco Zamponi¹

¹*Laboratoire de Physique de l'Ecole Normale Supérieure, ENS, Université PSL, CNRS, Sorbonne Université, Université de Paris, F-75005 Paris, France*

²*Université Paris-Saclay, CNRS, LPTMS, 91405, Orsay, France*

We present a numerical solution of the dynamical mean field theory of infinite-dimensional equilibrium liquids established in [Phys. Rev. Lett. **116**, 015902 (2016)]. For soft sphere interactions, we obtain the numerical solution by an iterative algorithm and a straightforward discretization of time. We also discuss the case of hard spheres, for which we first derive analytically the dynamical mean field theory as a non-trivial limit of the soft sphere one. We present numerical results for the memory function and the mean square displacement. Our results reproduce and extend kinetic theory in the dilute or short-time limit, while they also describe dynamical arrest towards the glass phase in the dense strongly-interacting regime.

Contents

I. Introduction	2
II. Dynamical mean field theory	2
A. General formulation	2
B. Adimensional equations	4
1. The Brownian case	4
2. The Newtonian case	4
C. Iterative solution	5
D. Dynamical glass transition	5
III. Hard Sphere limit	6
A. Brownian dynamics	6
B. Newtonian dynamics	8
C. Plateau equation	11
IV. Numerical algorithms	11
A. Solution scheme	11
B. Convergence algorithms	12
C. Dynamical equation in discrete time	13
1. Soft Spheres	13
2. Hard Spheres	13
V. Results	15
A. Soft Spheres	16
B. Brownian Hard Spheres	17
C. Newtonian Hard Spheres	18
VI. Conclusions	19
Acknowledgments	20
References	20
A. Some details on Newtonian dynamics	21
1. Distribution of the initial velocity	21
2. Viscosity	21
B. Brownian Hard Spheres	21

1. Derivation of the Laplace transform of the first iteration	21
2. Short-time behavior of the stress-stress correlation	22
C. Newtonian Hard Spheres	22
1. Short-time expansion from kinetic theory	22
2. Short-time expansion of the regular part of the memory function within DMFT	23
3. Low-density regime of the DMFT equations	24

I. INTRODUCTION

Solving the dynamics of equilibrium dense liquids is a notoriously difficult problem [1]. In the low-density limit, or at short times, the solution is obtained via kinetic theory, while at any density, hydrodynamics provides a description of the dynamics at large length and time scales. However, at high densities or low temperatures, kinetic theory breaks down, and the hydrodynamic regime is pushed to scales that are much larger than any experimentally relevant scale. In this strongly interacting “supercooled liquid” regime, dynamics is slow, viscosity is high, and both correlation functions and transport coefficients display non-trivial behavior that is neither captured by kinetic theory nor by hydrodynamics. The only microscopic description of this regime is obtained by the Mode-Coupling Theory (MCT) [2, 3], which is a set of closed equations derived from a series of poorly controlled approximations of the true dynamics. Despite its non-systematic nature [4–7], MCT accurately describes the initial slowing down of liquid dynamics upon supercooling, including the wavevector dependence of correlation functions [8].

Interestingly, in the formal limit in which the spatial dimension d goes to infinity, liquid thermodynamics reduces to the calculation of the second virial coefficient [9–12]. Based on this observation, a first attempt to solve exactly liquid dynamics for $d \rightarrow \infty$ was presented in [13] (see also [14]), but the full dynamical mean field theory (DMFT) that describes exactly the equilibrium dynamics in $d \rightarrow \infty$ was only derived recently, via a second-order virial expansion on trajectories [15] or via a dynamic cavity method [16, 17]. The DMFT provides a set of closed one-dimensional integro-differential equations, which exactly describe the many-body liquid dynamics in the thermodynamic limit, and are similar in structure to those obtained for quantum systems in the same limit [18]. We refer the reader to [17, 19–21] for a detailed review of the solution of liquid dynamics in infinite dimensions, including its extension to the out-of-equilibrium setting.

Unfortunately, the analytical solution of the DMFT equations is out of reach. In this work, we present their numerical solution, obtained through an iterative method and a straightforward discretization of time. This strategy, however, only works for differentiable interaction potentials. We thus discuss how to derive the DMFT of hard spheres via a non-trivial limit of a soft sphere interaction. We present numerical results for soft and hard spheres, supported by analytical computations at low densities, in the short time limit, and at long times in the glass phase.

The paper is organized as follows. In section II we review the basic equations of the DMFT of liquids. In section III, we discuss the Hard Sphere limit of DMFT. In section IV, we discuss the discretization and convergence algorithms used in this work. In section V, we present the numerical solution for Soft and Hard Spheres. Finally, in section VI we draw our conclusions and present some perspectives for future work. A few technical discussions are presented in Appendix.

II. DYNAMICAL MEAN FIELD THEORY

A. General formulation

In the following, we consider a liquid of interacting particles in d dimensions, with pair interaction potential $v(r)$ having a typical interaction scale ℓ , at temperature T and number density ρ in the thermodynamic limit. We denote by $\hat{\varphi} = 2^d \varphi/d = \rho V_d \ell^d/d$ the scaled packing fraction, where $V_d = \pi^{d/2}/\Gamma(1+d/2)$ is the volume of a unit sphere in d dimensions. In the infinite dimensional limit, it is convenient to describe the dynamics in terms of the inter-particle gap $h = d(r/\ell - 1)$, defining as well the rescaled potential $\bar{v}(h) = v[\ell(1+h/d)]$, which is assumed to have a well-defined limit when $d \rightarrow \infty$.

In the most general case, we consider the Langevin dynamics of the system, being $\hat{m} = (\ell^2/2d^2)m$ and $\hat{\zeta} = (\ell^2/2d^2)\zeta$ respectively the scaled mass and friction coefficient, which are kept finite in the limit $d \rightarrow \infty$ in order to obtain a non-trivial dynamics [15, 17]. Denoting a time derivative by a dot, $\dot{h}(t) = dh/dt$, DMFT leads to the following set of

self-consistent equations, which describe exactly the equilibrium dynamics when $d \rightarrow \infty$ [15–17, 21]:

$$\begin{aligned} \widehat{m}\ddot{h}(t) + \widehat{\zeta}\dot{h}(t) &= T - \bar{v}'(h(t)) - \beta \int_0^t du \mathcal{M}(t-u)\dot{h}(u) + \Xi(t) , \\ h(t=0) &= h_0 , \\ \dot{h}(t=0) &= \dot{h}_0 , \\ \langle \Xi(t)\Xi(u) \rangle &= 2\widehat{\zeta}T\delta(t-u) + \mathcal{M}(t-u) , \end{aligned} \quad (1)$$

where the memory kernel $\mathcal{M}(t)$ of the colored noise $\Xi(t)$ is determined by

$$\mathcal{M}(t) = \frac{\widehat{\varphi}}{2} \int d\dot{h}_0 \sqrt{\frac{\beta\widehat{m}}{2\pi}} e^{-\beta\widehat{m}\dot{h}_0^2/2} \int dh_0 e^{h_0 - \beta\bar{v}(h_0)} \bar{v}'(h_0) \langle \bar{v}'(h(t)) \rangle_{h_0, \dot{h}_0} , \quad (2)$$

where $\langle \cdot \rangle_{h_0, \dot{h}_0}$ is the average over the noise in the dynamical process starting in h_0 with velocity \dot{h}_0 (see Appendix A 1 for a discussion of the initial distribution of \dot{h}_0). The integrals over h_0 and \dot{h}_0 are performed over the real axis, as it will be implicitly understood for all the following integrals, whenever the integration bounds are not explicitly specified.

From the knowledge of the memory kernel $\mathcal{M}(t)$ one can derive all the dynamical observables, such as the scaled mean square displacement, $\frac{1}{N} \sum_i \langle |\mathbf{r}_i(t) - \mathbf{r}_i(0)|^2 \rangle = \ell^2 \Delta(t)/d$, which is the solution of the equation

$$\widehat{m}\ddot{\Delta}(t) + \widehat{\zeta}\dot{\Delta}(t) = T - \beta \int_0^t du \mathcal{M}(t-u)\dot{\Delta}(u) , \quad (3)$$

the associated scaled diffusion constant

$$\widehat{D} = \frac{2d^2}{\ell^2} D = \frac{T}{\widehat{\zeta} + \beta \int_0^\infty dt \mathcal{M}(t)} , \quad (4)$$

and the scaled shear viscosity (see Appendix A 2)

$$\frac{\widehat{\eta}_s}{\widehat{\varphi}} = \frac{\eta_s}{d\rho} = \frac{\beta\widehat{m}^2}{d} \int_0^\infty dt \ddot{\Delta}(t)^2 + \beta \int_0^\infty dt \mathcal{M}(t) . \quad (5)$$

We note that the kinetic contribution, i.e. the first term in Eq. (5), is subleading when $d \rightarrow \infty$ at constant density. However, it also diverges in the dilute limit $\rho \rightarrow 0$, in which the motion becomes ballistic, so it will be useful to keep this term to compare the DMFT results with finite-dimensional simulation data and with kinetic theory.

The DMFT equations (1) and (2) involve a potential term $\bar{v}'(h)$, a non-Markovian memory contribution from the integral term, and a Gaussian colored noise $\Xi(t)$. The goal of the present study is to determine $\mathcal{M}(t)$ as a self-consistent solution of these equations. The knowledge of $\mathcal{M}(t)$ is the fundamental step to compute the dynamical observables of the system as a function of the control parameters $\widehat{\varphi}, T$.

The physics of the system also strongly depends on the potential $\bar{v}(h)$. In the following, we will restrict ourselves to three kind of potentials: 1) a linear Soft Sphere (SSl) potential, $\bar{v}_{\text{SSl}}(h) = \varepsilon h \theta(-h)$; 2) a quadratic Soft Spheres (SSq) potential, $\bar{v}_{\text{SSq}}(h) = \varepsilon h^2 \theta(-h)/2$; 3) a Hard Sphere potential (HS), $\exp[-\bar{v}_{\text{HS}}(h)] = \theta(h)$, being $\theta(x)$ the Heaviside step function. All those potentials are short-ranged, with vanishing interaction for $h > 0$ (no overlap between particles), they are purely repulsive and both SSl and SSq tend to HS in the limit $\varepsilon \rightarrow \infty$. The energy scale ε gives the strength of the interactions, and its ratio with the temperature T will be one of the adimensional control parameters of our model.

It is clear that the DMFT equations, as written in Eqs. (1) and (2), cannot be straightforwardly applied to the HS case, in which the potential is not differentiable and the $\bar{v}'(h)$ terms appearing in Eqs. (1-2) are ill-defined. In section III, we will show how to regularize these equations to have a well-defined memory function $\mathcal{M}(t)$. The introduction of two kinds of soft sphere potentials (SSl and SSq) is motivated by the need of simple analytical calculations and unambiguous numerical solutions. Indeed, in section III we will show how the short-time or low-density limit of $\mathcal{M}(t)$ for Hard Spheres can be approached analytically, using the SSl potential for the sake of simplicity. Viceversa, the numerical solutions shown in section V A have been found with a SSq potential. The latter has a regular derivative in $h = 0$ - at variance with the SSl potential - and, therefore, the force changes continuously when particles get in contact and the numerical results are much clearer. Of course, the HS limit should not depend on the particular SS potential chosen.

B. Adimensional equations

We now briefly discuss what are the adimensional parameters that control the dynamical behavior, in the Brownian and Newtonian case, obtained as particular limits of the general Langevin dynamics. The discussion of the general (mixed) case is a straightforward extension of the ones below and is not reported for conciseness.

1. The Brownian case

In the Brownian (overdamped) case, one takes $\widehat{m} = 0$; the evolution equation (1) becomes then a first-order differential equation, so the initial condition on the velocity \dot{h}_0 disappears from the dynamics and from $\mathcal{M}(t)$ in Eq. (2). If $\widehat{m} = 0$, the characteristic time of Eq. (1) reads $\tau_B = \widehat{\zeta}/T$, which will be set to 1 in this case with the rescaling $t/\tau_B \rightarrow t$. The adimensional potential, memory kernel and noise are also rescaled as $\beta \bar{v}(h) \rightarrow \bar{v}(h)$, $\beta^2 \mathcal{M}(t\tau_B) \rightarrow \mathcal{M}(t)$ and $\beta \Xi(t\tau_B) \rightarrow \Xi(t)$. Substituting the rescaled variables into the dynamical evolution in Eq. (1) multiplied by β one gets

$$\begin{aligned} \dot{h}(t) &= 1 - \bar{v}'(h(t)) - \int_0^t du \mathcal{M}(t-u) \dot{h}(u) + \Xi(t) , \\ h(t=0) &= h_0 , \\ \langle \Xi(t)\Xi(u) \rangle &= 2\delta(t-u) + \mathcal{M}(t-u) , \end{aligned} \tag{6}$$

with the adimensional self-consistent equation:

$$\mathcal{M}(t) = \frac{\widehat{\varphi}}{2} \int dh_0 e^{h_0 - \bar{v}(h_0)} \bar{v}'(h_0) \langle \bar{v}'(h(t)) \rangle_{h_0} . \tag{7}$$

It is evident that the dynamics is then governed by two adimensional parameters only: the rescaled packing fraction $\widehat{\varphi}$ and the rescaled interaction strength or inverse temperature $\widehat{\varepsilon} = \beta\varepsilon$. Note that these rescalings are equivalent to setting $\ell = 1$, $\tau_B = 1$ and $\varepsilon = 1$ as units of length, time and energy, respectively.

2. The Newtonian case

Setting $\widehat{m} > 0$ and $\widehat{\zeta} = 0$ in the dynamical equations (1) gives Newtonian dynamics. The adimensionalisation can be done as in the Brownian case, but the characteristic time now reads $\tau_N = \sqrt{\widehat{m}/T}$ while the potential, memory and noise scale as in the Brownian case. For the initial velocity, one can define $\dot{h}_0 = g_0/\tau_N$, being g_0 a Gaussian variable of zero average and unit variance. Again, one substitutes the rescaled variables into the Newtonian dynamical equation (1) and gets

$$\begin{aligned} \ddot{h}(t) &= 1 - \bar{v}'(h(t)) - \int_0^t du \mathcal{M}(t-u) \dot{h}(u) + \Xi(t) , \\ h(t=0) &= h_0 , \\ \dot{h}(t=0) &= g_0 , \\ \langle \Xi(t)\Xi(u) \rangle &= \mathcal{M}(t-u) , \end{aligned} \tag{8}$$

with the adimensional self-consistent equation

$$\mathcal{M}(t) = \frac{\widehat{\varphi}}{2} \int \frac{dg_0}{\sqrt{2\pi}} e^{-g_0^2/2} \int dh_0 e^{h_0 - \bar{v}(h_0)} \bar{v}'(h_0) \langle \bar{v}'(h(t)) \rangle_{h_0, g_0} . \tag{9}$$

We emphasize that the Newtonian and Brownian equations have a similar structure, but the time scales are totally unrelated, as they depend on different physical coefficients. As in the Brownian case, the adimensional parameters characterizing the system are $\widehat{\varphi}$ and $\widehat{\varepsilon}$. The adimensionalisation is now equivalent to setting $\ell = 1$, $\tau_N = 1$ and $\varepsilon = 1$.

C. Iterative solution

As in the DMFT of quantum systems [18], finding $\mathcal{M}(t)$ for all times t by means of an analytical solution is beyond current possibilities. A numerical solution can be found, however, by means of the following iterative procedure: 1) define an initial memory kernel $\mathcal{M}(t) = 0$ (or any other more convenient initial condition); 2) simulate the stochastic trajectories $h(t)$ from Eq. (1) with $\mathcal{M}(t)$; 3) compute the new memory kernel $\mathcal{M}(t)$ through Eq. (2); 4) repeat until convergence is achieved. If the potential is differentiable, the above procedure can be implemented by a straightforward discretization of time.

The iterative procedure introduced above is, however, not guaranteed to be convergent. Still, we can observe that the self-consistent Eq. (2) takes the form $\mathcal{M} = \widehat{\varphi}\mathcal{F}_{\text{DMFT}}[\mathcal{M}]$, with an explicit factor of density in front of the implicit functional $\mathcal{F}_{\text{DMFT}}[\mathcal{M}]$. Hence, writing the memory kernel in a low density expansion as $\mathcal{M} = \widehat{\varphi}\mathcal{M}^{(1)} + \widehat{\varphi}^2\mathcal{M}^{(2)} + \dots$, the first-order term $\mathcal{M}^{(1)} = \widehat{\varphi}\mathcal{F}_{\text{DMFT}}[0]$ is precisely obtained by setting $\mathcal{M} = 0$ in the dynamical process, $\mathcal{M}^{(2)} = \widehat{\varphi}\mathcal{F}_{\text{DMFT}}[\mathcal{M}^{(1)}]$ is obtained by setting $\mathcal{M} = \mathcal{M}^{(1)}$, and so on, recursively. So, the solution of the iterative procedure after n iterations gives the low-density expansion of $\mathcal{M}(t)$ at order n , and the convergence of the iterative procedure is equivalent to the convergence of the low-density expansion.

D. Dynamical glass transition

The DMFT equations can exhibit a dynamically arrested phase, in which the memory function does not decay to zero but to a finite plateau, and the mean square displacement reaches a plateau without showing any diffusive regime. We briefly recall here how a closed equation for the plateau of $\mathcal{M}(t)$ can be derived, see [15, 17, 21] for details.

Let us assume that the memory can be decomposed into a constant component \mathcal{M}_∞ (the plateau) and a “fast” component $\mathcal{M}_f(t)$ that decays to zero over a finite time scale, i.e.

$$\mathcal{M}(t) = \mathcal{M}_\infty + \mathcal{M}_f(t) , \quad \lim_{t \rightarrow \infty} \mathcal{M}_f(t) = 0 . \quad (10)$$

Correspondingly, we can decompose the noise as $\Xi(t) = \Xi_f(t) + \Xi_\infty$, where the two components are independent and have variance $\langle \Xi_f(t)\Xi_f(u) \rangle = 2\widehat{C}T\delta(t-u) + \mathcal{M}_f(t-u)$ and $\langle \Xi_\infty^2 \rangle = \mathcal{M}_\infty$, respectively. Plugging this in Eq. (1), we obtain

$$\mathcal{L}[h] = T - \bar{v}'(h) - \beta\mathcal{M}_\infty(h - h_0) + \Xi_\infty = -w'(h) , \quad (11)$$

where $\mathcal{L}[h]$ is a dynamical operator that encodes all the time derivatives together with the fast components of the noise and friction. Because the noise and friction are in equilibrium at temperature T (i.e. they satisfy the fluctuation-dissipation theorem [22]), at long times the system equilibrates in the potential $w(h)$, thus reaching the conditional distribution

$$p(h|h_0, \Xi_\infty) = \frac{e^{-\beta w(h)}}{\int dz e^{-\beta w(z)}} , \quad w(h) = \bar{v}(h) - Th + \frac{\beta\mathcal{M}_\infty}{2}(h - h_0)^2 - \Xi_\infty h . \quad (12)$$

The presence of a finite plateau adds a harmonic trap to the potential, which confines the particle in a finite region and prevents diffusion. Taking the limit $t \rightarrow \infty$ of Eq. (2), we have

$$\langle \bar{v}'(h(t)) \rangle_{h_0, h_0} \rightarrow \int d\Xi_\infty p(\Xi_\infty) \int dh p(h|h_0, \Xi_\infty) \bar{v}'(h) , \quad (13)$$

where $p(\Xi_\infty)$ is a Gaussian with zero mean and variance \mathcal{M}_∞ . This gives a closed equation for \mathcal{M}_∞ in the form

$$\mathcal{M}_\infty = \widehat{\varphi} \int dh_0 e^{h_0 - \beta \bar{v}(h_0)} \bar{v}'(h_0) \int d\Xi_\infty p(\Xi_\infty) \int dh p(h|h_0, \Xi_\infty) \bar{v}'(h) . \quad (14)$$

Note that one of the three integrals can be eliminated by some simple manipulation [16, 21]. At low density or high temperature, Eq. (14) admits $\mathcal{M}_\infty = 0$ as unique solution; at high density or low temperature, instead, a finite solution $\mathcal{M}_\infty > 0$ appears, usually in a discontinuous way. The line in the temperature-density plane separating the two situations is called the “dynamical glass transition line”, $\widehat{\varphi}_d(T)$. Note that the long time distribution in Eq. (12) does not depend on the details of the short-time dynamics, encoded in $\mathcal{L}[h]$, provided the equilibrium conditions are satisfied. As a result, the plateau equation is the same for Brownian and Newtonian dynamics.

III. HARD SPHERE LIMIT

In this section, we derive the DMFT for Hard Spheres, by taking the $\hat{\varepsilon} \rightarrow \infty$ limit of the DMFT equations for the SSL potential. We discuss separately the Brownian and Newtonian cases because the physical and mathematical properties of the equations are very different in the two cases.

A. Brownian dynamics

Recall that we work here in dimensionless units as discussed in section IIB1. For a Brownian SSL system, the DMFT equations (6-7) become

$$\begin{aligned} \dot{h}(t) &= 1 + \hat{\varepsilon}\theta(-h(t)) - \int_0^t du \mathcal{M}(t-u)\dot{h}(u) + \Xi(t) , \\ h(t=0) &= h_0 , \\ \langle \Xi(t)\Xi(u) \rangle &= 2\delta(t-u) + \mathcal{M}(t-u) , \end{aligned} \quad (15)$$

with

$$\mathcal{M}(t) = \frac{\hat{\varphi}}{2} \int_{-\infty}^0 dh_0 e^{h_0 + \hat{\varepsilon}h_0} \hat{\varepsilon}^2 G(h_0, t) , \quad G(h_0, t) = \langle \theta(-h(t)) \rangle_{h_0} , \quad (16)$$

where $G(h_0, t)$ is the probability for the dynamical process starting at h_0 to end at any $h < 0$ at time t . Note that the factor $\hat{v}'(h_0)$ enforces the condition $h_0 < 0$ in the memory function.

To gain some insight on the $\hat{\varepsilon} \rightarrow \infty$ limit, we will begin by considering the first iteration of the algorithm described in section IIC, which corresponds to setting $\mathcal{M}(t) = \mathcal{M}^{(0)}(t) \equiv 0$ in Eq. (15). We then have

$$\dot{h}(t) = 1 + \hat{\varepsilon}\theta(-h(t)) + \Xi(t) , \quad \langle \Xi(t)\Xi(u) \rangle = 2\delta(t-u) , \quad (17)$$

and we want to compute $G(h_0, t)$, which follows the backward Kolmogorov evolution equation (see e.g. [23])

$$\begin{aligned} \dot{G}(h_0, t) &= G''(h_0, t) + (1 + \hat{\varepsilon})G'(h_0, t) , & h_0 < 0 , \\ \dot{G}(h_0, t) &= G''(h_0, t) + G'(h_0, t) , & h_0 > 0 , \end{aligned} \quad (18)$$

where primes denote derivatives with respect to h_0 , and with boundary conditions

$$G(h_0, t=0) = \theta(-h_0) , \quad G(h_0 \rightarrow -\infty, t) = 1 , \quad G(h_0 \rightarrow \infty, t) = 0 . \quad (19)$$

The evolution of $G(h_0, t)$ can be solved in Laplace space. We solve Eq. (18) for $h_0 < 0$ and $h_0 > 0$ separately and then impose the continuity of $G(h_0, t)$ and $G'(h_0, t)$ at $h_0 = 0$ (see Appendix B1), getting

$$\begin{aligned} \tilde{G}(h_0, s) &= \begin{cases} \frac{1}{s} + c_-(s)e^{\lambda_-(s)h_0} , & h_0 < 0 , \\ c_+(s)e^{\lambda_+(s)h_0} , & h_0 > 0 , \end{cases} \\ \lambda_-(s) &= \frac{1}{2} \left(-1 - \hat{\varepsilon} + \sqrt{(1 + \hat{\varepsilon})^2 + 4s} \right) , & c_-(s) = \frac{\lambda_+(s)}{s[\lambda_-(s) - \lambda_+(s)]} , \\ \lambda_+(s) &= \frac{1}{2} \left(-1 - \sqrt{1 + 4s} \right) , & c_+(s) = \frac{\lambda_-(s)}{s[\lambda_-(s) - \lambda_+(s)]} . \end{aligned} \quad (20)$$

The Laplace transform of $\mathcal{M}^{(1)}(t)$, corresponding to the first iteration (or first-order in density), is therefore

$$\tilde{\mathcal{M}}^{(1)}(s) = \frac{\hat{\varphi}}{2} \int_{-\infty}^0 dh_0 e^{h_0 + \hat{\varepsilon}h_0} \hat{\varepsilon}^2 \tilde{G}(h_0, s) = \frac{\hat{\varphi}}{2} \hat{\varepsilon}^2 \left[\frac{1}{s(1 + \hat{\varepsilon})} + \frac{c_-(s)}{1 + \hat{\varepsilon} + \lambda_-(s)} \right] . \quad (21)$$

Note that from $\tilde{\mathcal{M}}^{(1)}(s)$ we immediately get the lowest order density correction to the diffusion constant via Eq. (4):

$$\tilde{\mathcal{M}}^{(1)}(s=0) = \frac{\hat{\varphi}}{2} \frac{\hat{\varepsilon}^2(2 + \hat{\varepsilon})}{(1 + \hat{\varepsilon})^3} \quad \Rightarrow \quad \hat{D}^{(1)} = \frac{1}{1 + \frac{\hat{\varphi}}{2} \frac{\hat{\varepsilon}^2(2 + \hat{\varepsilon})}{(1 + \hat{\varepsilon})^3}} , \quad (22)$$

which in the HS limit reads

$$\widehat{D}_{\text{HS}}^{(1)} = \lim_{\widehat{\varepsilon} \rightarrow \infty} \widehat{D}^{(1)}(\widehat{\varepsilon}) = \frac{1}{1 + \frac{\widehat{\varphi}}{2}}. \quad (23)$$

The HS limit of the Laplace transform in Eq. (21) can be inverted analytically, yielding

$$\widetilde{\mathcal{M}}_{\text{HS}}^{(1)}(s) = \frac{\widehat{\varphi}}{1 + \sqrt{1 + 4s}} \quad \Rightarrow \quad \mathcal{M}_{\text{HS}}^{(1)}(t) = \frac{\widehat{\varphi}}{2} \left[\frac{e^{-t/4}}{\sqrt{\pi t}} - \frac{1}{2} \operatorname{erfc}(\sqrt{t}/2) \right], \quad (24)$$

where $\operatorname{erfc}(x) = 1 - \operatorname{erf}(x)$ is the complementary error function. We stress that this is not yet the solution of the dynamical equations (15-16), because we performed only one iteration, which corresponds to the lowest order expansion in $\widehat{\varphi}$. However, Eq. (24) provides an important information: for Brownian Hard Spheres, $\mathcal{M}(t) \sim \widehat{\varphi}/\sqrt{4\pi t}$ is divergent for small times $t \rightarrow 0$. Because in the $d \rightarrow \infty$ limit the memory function also corresponds to the stress autocorrelation [15, 21], this result is in agreement with the exact short-time behavior of the stress autocorrelation of Brownian Hard Spheres, as obtained from kinetic theory [24–26] (see Appendix B 2). Note that the divergence is integrable, and it is thus consistent with a liquid phase having finite diffusivity.

Based on the above results, and on physical intuition, we conjecture that the Brownian HS dynamics is described by the process

$$\begin{aligned} \dot{h}(t) &= 1 - \int_0^t du \mathcal{M}(t-u) \dot{h}(u) + \Xi(t), \\ h(t=0) &= 0, \\ \langle \Xi(t) \Xi(u) \rangle &= 2\delta(t-u) + \mathcal{M}(t-u), \\ \mathcal{M}(t) &= \frac{\widehat{\varphi}}{2} p(0, t|0), \end{aligned} \quad (25)$$

where the process is restricted to $h > 0$ with reflecting boundary conditions in $h = 0$. We call $p(h, t|h_0)$ its propagator, i.e. the probability of starting in h_0 at time $t = 0$ and arriving in h after a time t . The problem of computing $\mathcal{M}(t)$ then reduces to the computation of the return probability $p(0, t|0)$ for the stochastic process defined in (25).

To support this conjecture, we first note that it is consistent with the exact analysis of the first iteration, as given in Eq. (24). Indeed, assuming $\mathcal{M}^{(0)}(t) \equiv 0$, the propagator of a Brownian motion with drift and reflecting barrier in $h = 0$ is exactly known [27, Appendix 1.16, p. 133], and one finds

$$p^{(0)}(0, t|0) = \frac{e^{-t/4}}{\sqrt{\pi t}} - \frac{1}{2} \operatorname{erfc}(\sqrt{t}/2) \quad \Rightarrow \quad \mathcal{M}^{(1)}(t) = \frac{\widehat{\varphi}}{2} p^{(0)}(0, t|0). \quad (26)$$

A second and more precise argument, valid to all orders in density, is as follows. We start from the exact formula for $\mathcal{M}(t)$ in Eq. (16), where

$$G(h_0, t) = \langle \theta(-h) \rangle_{h_0} = \int_{-\infty}^0 dh p_{\widehat{\varepsilon}}(h, t|h_0), \quad (27)$$

and $p_{\widehat{\varepsilon}}(h, t|h_0)$ is the propagator in the presence of the SSI potential. We first perform the change of variable $x = \widehat{\varepsilon}h$ to obtain

$$\mathcal{M}(t) = \frac{\widehat{\varphi}}{2} \int_{-\infty}^0 dx e^{\frac{x}{\widehat{\varepsilon}} + x} \widehat{\varepsilon} G\left(\frac{x}{\widehat{\varepsilon}}, t\right) \underset{\widehat{\varepsilon} \rightarrow \infty}{\approx} \frac{\widehat{\varphi}}{2} \int_{-\infty}^0 dx e^x \widehat{\varepsilon} G(0, t) = \frac{\widehat{\varphi}}{2} \widehat{\varepsilon} G(0, t). \quad (28)$$

We now need to estimate $G(0, t) = \int_0^{\infty} dh p_{\widehat{\varepsilon}}(h, t|0)$ in the limit $\widehat{\varepsilon} \rightarrow \infty$. In the presence of a strongly repulsive potential $\bar{v}(h) = -\widehat{\varepsilon}h$ for negative h , it is clear that the trajectories that contribute to this integral start from $h_0 = 0$, stay on the positive side up to time t^- and end up on the negative side at some typical value $h < 0$ such that $h \sim \mathcal{O}(1/\widehat{\varepsilon})$ or $\widehat{\varepsilon}h \sim \mathcal{O}(1)$. Hence, it is reasonable to assume that on the negative side we have $p_{\widehat{\varepsilon}}(h, t|0) \sim p_{\widehat{\varepsilon}}(0, t|0) A(\widehat{\varepsilon}h)$. It is also natural to expect that the function $A(x)$ is independent of time and of density, as it only depends on the short time dynamics and on how far the particle can penetrate on the negative axis in the presence of $\bar{v}(h)$. Therefore one has

$$G(0, t) = \int_{-\infty}^0 dh p_{\widehat{\varepsilon}}(h, t|0) \underset{\widehat{\varepsilon} \rightarrow \infty}{\approx} p_{\widehat{\varepsilon} \rightarrow \infty}(0, t|0) \int_{-\infty}^0 dh A(\widehat{\varepsilon}h) \underset{\widehat{\varepsilon} \rightarrow \infty}{\approx} \frac{A}{\widehat{\varepsilon}} p_{\widehat{\varepsilon} \rightarrow \infty}(0, t|0), \quad (29)$$

where $\mathcal{A} = \int_{-\infty}^0 dx A(x)$. In the limit $\hat{\varepsilon} \rightarrow \infty$, because of the repulsive potential, the particle gets immediately reflected on the positive axis as soon as it touches $h = 0^-$: therefore $p_{\hat{\varepsilon} \rightarrow \infty}(0, t|0)$ coincides with the propagator $p(0, t|0)$ of the stochastic process in the presence of a reflecting boundary at the origin. Combining Eq. (28) and (29) we obtain

$$\mathcal{M}_{\text{HS}}(t) = \frac{\hat{\varphi}}{2} \mathcal{A} p(0, t|0) , \quad (30)$$

where we have argued that \mathcal{A} is time-dependent. Its value can thus be fixed by the low-density approximation, for which we can explicitly compute $\mathcal{A} = 1$.

In conclusion, we have shown that the DMFT equations for infinite dimensional Brownian Hard Spheres are those given in Eq. (25).

B. Newtonian dynamics

In order to approach the HS limit of the Newtonian dynamical Eqs. (8-9), we will proceed in several steps. First, using a SSL potential, the purely Newtonian dynamics reads

$$\begin{aligned} \ddot{h}(t) &= 1 + \hat{\varepsilon} \theta(-h(t)) - \int_0^t du \mathcal{M}(t-u) \dot{h}(u) + \Xi(t) , \\ h(t=0) &= h_0 , \\ \dot{h}(t=0) &= g_0 , \\ \langle \Xi(t) \Xi(u) \rangle &= \mathcal{M}(t-u) , \end{aligned} \quad (31)$$

with the self-consistent condition on the memory function

$$\mathcal{M}(t) = \frac{\hat{\varphi}}{2} \int_{-\infty}^{\infty} \frac{dg_0}{\sqrt{2\pi}} e^{-g_0^2/2} \int_{-\infty}^0 dh_0 e^{h_0 + \hat{\varepsilon} h_0} \hat{\varepsilon}^2 \langle \theta(-h(t)) \rangle_{h_0, g_0} . \quad (32)$$

Setting $\mathcal{M}^{(0)}(t) \equiv 0$, the dynamics in Eq. (31) becomes deterministic. In the absence of memory, particles follow a piecewise uniformly accelerated motion, with acceleration equal to 1 for $h > 0$ and to $1 + \hat{\varepsilon}$ for $h < 0$. Therefore, the only trajectories contributing to $\mathcal{M}(t)$ in Eq. (32) are those starting with $h_0 < 0$, moving across the negative side until they reach $h = 0$, and leaving it with positive velocity after the given time t . Once a trajectory has left the negative side, it will never return to the origin in the absence of noise. The condition $h(t) < 0$ then becomes equivalent to $h_0 + g_0 t + (1 + \hat{\varepsilon})t^2/2 < 0$. The integral in (32) can thus be analytically computed and gives

$$\mathcal{M}^{(1)}(t) = \frac{\hat{\varphi}}{2} \int_{-\infty}^{\infty} \frac{dg_0}{\sqrt{2\pi}} e^{-g_0^2/2} \int_{-\infty}^{\min(0, -g_0 t - (1 + \hat{\varepsilon})t^2/2)} dh_0 e^{h_0 + \hat{\varepsilon} h_0} \hat{\varepsilon}^2 = \hat{\varphi} \frac{\hat{\varepsilon}^2}{1 + \hat{\varepsilon}} \Theta \left(-\frac{1 + \hat{\varepsilon}}{2} t \right) , \quad (33)$$

being $\Theta(x) = \int_{-\infty}^x dz e^{-z^2/2} / \sqrt{2\pi}$ the normal cumulative distribution function. In the HS limit $\hat{\varepsilon} \rightarrow \infty$, one finds

$$\mathcal{M}_{\text{HS}}^{(1)}(t) = \sqrt{\frac{8}{\pi}} \hat{\varphi} \delta(t) . \quad (34)$$

This result has a clear physical interpretation: in the absence of noise (coming from the self-consistent bath of surrounding particles) it is impossible to have multiple collisions, and the first iteration outcome thus consists of the force-force correlation during the first (and only) collision that the particles are possibly undergoing. This correlation decays over time scales of order $1/\hat{\varepsilon}$, and it is delta-peaked in the HS limit as one expects for instantaneous collisions. The same result can be computed for the SSq potential, leading to a memory function which is different from Eq. (33) but which, as expected, also converges to Eq. (34) in the HS limit. From the first iteration one can also compute the diffusion coefficient $\hat{D}^{(1)}$, which for Newtonian HS reads

$$\hat{D}_{\text{HS}}^{(1)} = \left[\int_0^{\infty} \mathcal{M}(t) dt \right]^{-1} = \sqrt{\frac{\pi}{2}} \frac{1}{\hat{\varphi}} . \quad (35)$$

We conclude that, at the lowest order in density, the effect of particle collisions in the HS limit is to add a white noise to the deterministic, Newtonian motion.

The presence of a delta function in the stress-stress correlation (which coincides with the memory function in infinite dimensions) is well known from kinetic theory [26, 28, 29]. The coefficient of the delta function is given by $2/\widehat{D}_{\text{HS}}^{(1)}$, as derived above, and $\widehat{D}_{\text{HS}}^{(1)}$ coincides with the first-order Enskog coefficient for hard spheres at $d = \infty$ [1, 30–32], see Appendix C 1 for details. The short time expansion in any dimension also shows that

$$\mathcal{M}_{\text{HS}}(t) = 2\zeta_0 \delta(t) + B + Ct + \dots, \quad \zeta_0 = \sqrt{\frac{2}{\pi}} \widehat{\varphi} = \frac{1}{\widehat{D}_{\text{HS}}^{(1)}}, \quad (36)$$

but the coefficient B vanishes when $d \rightarrow \infty$, see Appendix C 1 for a detailed discussion. Hence, the memory function is expected to be the sum of a delta function and a regular part that vanishes linearly at short times.

Based on these observations, we conjecture that the memory function time scales separate for large $\widehat{\varepsilon}$, namely

$$\mathcal{M}(t) \sim 2\zeta_0 \widehat{\varepsilon} \mathcal{M}_{\text{sing}}(t\widehat{\varepsilon}) + \mathcal{M}_{\text{reg}}(t), \quad \int_{-\infty}^{\infty} dt \mathcal{M}_{\text{sing}}(t) = 1, \quad (37)$$

where the first term becomes a delta function for $\widehat{\varepsilon} \rightarrow \infty$, and the second term is not singular. Because at short times the motion is ballistic and dominated by the initial velocity, the regular part of the memory function plays no role, and at all orders in density we expect the result of the first iteration to remain correct, hence $\zeta_0 = \sqrt{2/\pi} \widehat{\varphi}$, in agreement with kinetic theory. On the other hand, for the calculation of the regular part of the memory, we can safely consider $\mathcal{M}_{\text{sing}}(t)$ to be a delta function when $\widehat{\varepsilon}$ is large enough. We can thus write the effective process as

$$\begin{aligned} \ddot{h}(t) + \zeta_0 \dot{h}(t) &= 1 + \widehat{\varepsilon} \theta(-h(t)) - \int_0^t du \mathcal{M}_{\text{reg}}(t-u) \dot{h}(u) + \Xi(t), \\ \langle \Xi(t) \Xi(u) \rangle &= 2\zeta_0 \delta(t-u) + \mathcal{M}_{\text{reg}}(t-u), \end{aligned} \quad (38)$$

in which ζ_0 plays the role of an effective friction coefficient and white noise term.

At very short times, the motion is given, for large $\widehat{\varepsilon}$, by

$$h(t) = h_0 + g_0 t + \frac{1}{2} \widehat{\varepsilon} t^2 + \mathcal{O}(\sqrt{\zeta_0} t^{3/2}). \quad (39)$$

Because the typical initial condition is $h_0 = -u_0/\widehat{\varepsilon}$ with $u_0 \sim \mathcal{O}(1)$, the trajectory exits from the negative side at a time t_{ex} with velocity g_{ex} , given respectively by

$$t_{ex} = \frac{-g_0 + \sqrt{g_0^2 + 2u_0}}{\widehat{\varepsilon}}, \quad g_{ex} = \sqrt{g_0^2 + 2u_0} \geq 0. \quad (40)$$

Note that the term $\mathcal{O}(\sqrt{\zeta_0} t^{3/2})$ in Eq. (39) gives a subleading correction that can be neglected because $t \sim 1/\widehat{\varepsilon}$. The motion for $t < t_{ex} \rightarrow 0$ in the region $h < 0$ contributes to the delta peak and is not affected by noise, while the motion for $t > t_{ex}$ contributes to the regular part of the memory function. For the calculation of the regular part of the memory function, we can thus consider that trajectories start at $t = 0$ in $h_0 = 0$ with initial postcollisional - i.e. positive - velocity g_{ex} given in Eq. (40). We thus need to compute the initial distribution of g_{ex} . The initial distribution of (h_0, g_0) is, for large $\widehat{\varepsilon}$,

$$p(h_0, g_0) = \frac{1}{\sqrt{2\pi}} e^{-g_0^2/2} e^{\widehat{\varepsilon} h_0} \widehat{\varepsilon} \theta(-h_0), \quad (41)$$

which implies

$$p_{ex}(g_{ex}) = \int dh_0 dg_0 p(h_0, g_0) \delta\left(g_{ex} - \sqrt{g_0^2 - 2\widehat{\varepsilon} h_0}\right) = 2g_{ex}^2 \frac{1}{\sqrt{2\pi}} e^{-g_{ex}^2/2}. \quad (42)$$

To summarize, we can now consider $g_{ex} \rightarrow g_0$ as the initial velocity, with $h_0 = 0$, and write the regular part from Eq. (32) as

$$\mathcal{M}_{\text{reg}}(t) = \frac{\widehat{\varphi}}{2} \int_0^{\infty} dg_0 p_{ex}(g_0) \lim_{\widehat{\varepsilon} \rightarrow \infty} \widehat{\varepsilon} \langle \theta(-h(t)) \rangle_{h_0=0, g_0}, \quad (43)$$

where the trajectories evolve according to Eq. (38) in the large $\widehat{\varepsilon}$ limit. Physically, while the singular memory contribution is given by the instantaneous collisions, the regular part is counting how many trajectories starting after

a collision at $t = 0$ with postcollisional velocity g_0 will come back to collide again at finite time $t > 0$ because of the noise.

Finally, we need to treat the collision with the barrier that appears at time t in Eq. (43). The trajectory starts in $h_0 = 0$ with velocity $g_0 \geq 0$ and can undergo multiple collisions in $[0, t]$. We are interested in trajectories that are negative at time t , so let us call t_1 the time at which $h(t_1) = 0$ for the last time, and $g_1 = \dot{h}(t_1)$ the velocity at that time. We can assume that the colliding motion between t_1 and t is again dominated by the deterministic part, as in Eq. (39); then, this motion is statistically independent from what happened before t_1 , and we can write

$$\langle \theta(-h(t)) \rangle_{0, g_0} = \int_{-\infty}^0 dg_1 \int_0^t dt_1 f(g_1, t_1 | g_0) P_{\hat{\varepsilon}}(t - t_1 | g_1), \quad (44)$$

where

- $f(g_1, t_1 | g_0) dt_1 dg_1$ is the return probability to $h = 0$ at a time $\in [t_1, t_1 + dt_1]$ with (negative) velocity $\in [g_1, g_1 + dg_1]$. Note that this probability can also be expressed in terms of the probability $p(g_1, h_1, t | g_0) dg_1 dh_1$, which is the probability of finding the particle at time t in a point $\in [h_1, h_1 + dh_1]$ with velocity $\in [g_1, g_1 + dg_1]$, for the limiting process, which is restricted to $h \geq 0$ with a reflecting barrier in $h = 0$ [33, 34]. The relation between $f(g_1, t_1 | g_0)$ and the propagator $p(g_1, h_1, t | g_0)$ reads [33, 34]

$$f(g_1, t_1 | g_0) = |g_1| p(g_1, 0, t_1 | g_0), \quad g_1 \leq 0. \quad (45)$$

Indeed, every particle that at time t_1 is in $h \in [0, |g_1| dt_1]$ will be found in $h = 0$ in a time $t \in [t_1, t_1 + dt_1]$.

- $P_{\hat{\varepsilon}}(t - t_1 | g_1)$ is the probability that $h(t) \leq 0$, given that the trajectory has $h(t_1) = 0$ and $g(t_1) = g_1$. This quantity is immediately computed because

$$h(t) = g_1(t - t_1) + \frac{\hat{\varepsilon}}{2}(t - t_1)^2 \leq 0 \quad \Leftrightarrow \quad t + \frac{2g_1}{\hat{\varepsilon}} \leq t_1 \leq t. \quad (46)$$

We thus obtain $P_{\hat{\varepsilon}}(t - t_1 | g_1) = \theta\left(t + \frac{2g_1}{\hat{\varepsilon}} \leq t_1 \leq t\right)$.

Hence,

$$\hat{\varepsilon} \langle \theta(-h(t)) \rangle_{0, g_0} = \hat{\varepsilon} \int_{-\infty}^0 dg_1 \int_{t + \frac{2g_1}{\hat{\varepsilon}}}^t dt_1 f(g_1, t_1 | g_0) \approx \int_{-\infty}^0 dg_1 2|g_1| f(g_1, t | g_0) = \int_{-\infty}^0 dg_1 2g_1^2 p(g_1, 0, t | g_0). \quad (47)$$

Plugging this in Eq. (43), we obtain that

$$\mathcal{M}_{\text{reg}}(t) = \frac{\hat{\varphi}}{2} \int_0^{\infty} dg_0 2g_0^2 \frac{1}{\sqrt{2\pi}} e^{-g_0^2/2} \int_{-\infty}^0 dg_1 2g_1^2 p(g_1, 0, t | g_0), \quad (48)$$

which is well defined and regular in the HS limit $\hat{\varepsilon} \rightarrow \infty$.

In conclusion, we have shown that infinite dimensional Newtonian Hard Spheres are described by the simple DMFT equations

$$\begin{aligned} \ddot{h}(t) + \zeta_0 \dot{h}(t) &= 1 - \int_0^t du \mathcal{M}_{\text{reg}}(t - u) \dot{h}(u) + \Xi(t), \\ h(t = 0) &= 0, \\ \dot{h}(t = 0) &= g_0, \\ \langle \Xi(t) \Xi(u) \rangle &= 2\zeta_0 \delta(t - u) + \mathcal{M}_{\text{reg}}(t - u). \end{aligned} \quad (49)$$

with a reflecting (elastic) barrier at $h = 0$, $\zeta_0 = \sqrt{2/\pi} \hat{\varphi}$ and the self-consistent condition (48) for the regular part of the memory kernel. A short time expansion of Eqs. (49) shows that $\mathcal{M}_{\text{reg}}(t) \sim Ct$ at short times, hence in Eq. (36) the coefficient $B = 0$ consistently with the kinetic theory expression. Furthermore, we obtain an analytic expression of the coefficient $C = 0.1578 \cdot \hat{\varphi}^3$, which to the best of our knowledge has not been obtained via kinetic theory. See Appendix C 2 for details.

C. Plateau equation

We now check that the DMFT equations for Hard Spheres give the correct equation for the plateau of the memory function in the glass phase, as derived from a thermodynamic analysis [21]. With the same decomposition of $\mathcal{M}(t)$ and $\Xi(t)$ as in section IID, we obtain

$$\mathcal{L}[h] = 1 - \mathcal{M}_\infty h(t) + \Xi_\infty = -w'(h) , \quad (50)$$

recalling that for Hard Spheres $h_0 = 0$, and that here we are using adimensional equations. Because there is a reflecting barrier in $h = 0$, the long time distribution is

$$p(h|\Xi_\infty) = \frac{e^{-w(h)}\theta(h)}{\int_0^\infty dz e^{-w(z)}} , \quad w(h) = -h + \frac{\mathcal{M}_\infty}{2}h^2 - \Xi_\infty h . \quad (51)$$

In the Brownian case, the long-time limit of the memory function is given by

$$\mathcal{M}_\infty = \frac{\hat{\varphi}}{2} p(0, t \rightarrow \infty | 0) = \frac{\hat{\varphi}}{2} \int d\Xi_\infty p(\Xi_\infty) p(0|\Xi_\infty) = \frac{\hat{\varphi}}{2} \int d\Xi_\infty p(\Xi_\infty) \frac{1}{\int_0^\infty dh e^{h - \frac{\mathcal{M}_\infty}{2}h^2 + \Xi_\infty h}} , \quad (52)$$

which provides a simple self-consistent equation for \mathcal{M}_∞ , recalling that $p(\Xi_\infty)$ is a Gaussian with zero mean and variance \mathcal{M}_∞ . In the Newtonian case, the distribution of $p(g, h, t|g_0)$ at long times is given by $p(h|\Xi_\infty)p(g)$, where $p(g)$ is a centered unit Gaussian. Plugging this in Eq. (48), the integrals over g_0 and g_1 evaluate to one, and we obtain the same result as in the Brownian case. Note that Eq. (52) is indeed the Hard Sphere limit of Eq. (13), as one can check explicitly using the SSL potential in Eq. (13) and taking the limit $\hat{\varepsilon} \rightarrow \infty$. The plateau Eq. (52) admits only the liquid solution $\mathcal{M}_\infty = 0$ for $\hat{\varphi} < 4.8067\dots$ and admits a non-trivial solution $\mathcal{M}_\infty > 0$ for $\hat{\varphi} > 4.8067\dots$ [21].

IV. NUMERICAL ALGORITHMS

In this section, we give some details on how to compute $\mathcal{M}(t)$ through the numerical integration of the stochastic differential equations discussed in the previous sections. The numerical scheme relies on stochastic differential equations and dynamical mean field theory, and is close to the approach used in [35].

A. Solution scheme

In order to compute $\mathcal{M}(t)$ numerically, one needs to solve the stochastic process in Eq. (1), in proper units as discussed in section IIB. For numerical convenience, we used the quadratic (harmonic) Soft Sphere potential (SSq), $\bar{v}(h) = \hat{\varepsilon}h^2\theta(-h)/2$, where $\theta(x)$ denotes the Heaviside step function. This potential reduces to the hard sphere potential when $\hat{\varepsilon} \rightarrow \infty$, it has a continuous derivative in $h = 0$, and it grows quickly when $h \rightarrow -\infty$. This choice allows one to restrict the integration over h_0 to a small region, because only the terms with $h_0 < 0$ contribute to Eq. (2), and those are weighted by a Gaussian-shaped distribution, namely

$$\mathcal{M}(t) = \frac{\hat{\varphi}}{2} \hat{\varepsilon}^2 \int_{-\infty}^{\infty} \frac{dg_0}{\sqrt{2\pi}} e^{-g_0^2/2} \int_{-\infty}^0 dh_0 e^{h_0 - \hat{\varepsilon}h_0^2/2} h_0 \langle h(t)\theta(-h(t)) \rangle_{h_0, g_0} . \quad (53)$$

The integrals in Eq. (53) are numerically computed by running trajectories starting in $h_{\min} < h_0 < 0$, with a typical cut-off $h_{\min} = -5/\sqrt{\hat{\varepsilon}}$, and drawing a random Gaussian initial velocity g_0 in the Newtonian case. Conversely, in the Hard Sphere case one needs to compute $\mathcal{M}(t)$ through Eqs. (25) or (48). Therefore, all the trajectories start at $h_0 = 0$ (postcollisional condition), with a g_0 distributed according to Eq. (42) in the Newtonian case.

Being at equilibrium, the system is time-translational invariant (TTI) and this property can be exploited to generate the correlated noise; indeed, if the noise correlation $\mathcal{K}(t)$ is TTI, the associated noise will be delta-correlated in frequency, namely $\langle \Xi(\omega)\Xi^*(\omega') \rangle = \mathcal{K}(\omega)\delta(\omega - \omega')$. One can generate independently the noise in Fourier space, $\Xi(\omega)$, with zero mean and variance $\mathcal{K}(\omega)$, and its inverse Fourier transform thus generates a correlated Gaussian noise $\Xi(t)$ with the desired correlation $\langle \Xi(t)\Xi(t') \rangle = \mathcal{K}(t - t')$. Note that, depending on the context, the white noise part can be generated independently and $\mathcal{K}(t) = \mathcal{M}(t)$, or it can be included in the Fourier transform and $\mathcal{K}(t) = 2\delta(t) + \mathcal{M}(t)$. The noise is generated at the beginning and it is then injected in the equation of motion for $h(t)$, which is then integrated to obtain the trajectory.

The iterations stop when a convergence criterion is reached: in our algorithm, we typically required that the rescaled viscosity $\hat{\eta}_s \propto \int_0^\infty \mathcal{M}(t) dt$ does not change significantly between iterations i and $i+1$, namely $|(\hat{\eta}_s^{i+1} - \hat{\eta}_s^i)/\hat{\eta}_s^i| < \delta$, where δ is a small parameter fixing the relative error. Obviously, many other convergence criteria can be chosen and some others have been tested to ensure that the results do not depend significantly on this arbitrary choice. We typically report numerical solutions with $\delta = 10^{-3}$, which is a compromise between a satisfyingly low relative error and a reasonable number of trajectories being needed to reduce fluctuations. One can also achieve smaller values of δ by increasing the number of trajectories while approaching convergence, which however increases the convergence time.

B. Convergence algorithms

The convergence algorithm discussed in section II C has been implemented on a fixed time grid, which yields a solution for $\mathcal{M}_n = \mathcal{M}(n\Delta t)$ with $0 \leq t < t_{\max} = N_S \Delta t$, being N_S the total number of time steps. This is the most straightforward way to approach the problem, but the maximum value of N_S is constrained by the computation of the retarded friction in Eq. (1), which has a time complexity scaling as N_S^2 .

More sophisticated algorithms can be developed to improve the computational efficiency and at the same time check the validity of the results. The main observation is that the DMFT equations are causal, i.e. the solution \mathcal{M}_n is independent on future times $m\Delta t > n\Delta t$. One can then compute a solution up to a final time t_1 , then fix the value of $\mathcal{M}(t)$ for $0 \leq t < t_1$ and extend a trajectory up to $t_2 > t_1$, compute $\mathcal{M}(t)$ in the new time window and so on. In our study, we also developed two algorithms exploiting causality: a step-by-step algorithm and a decimation algorithm.

The step-by-step algorithm computes recursively \mathcal{M}_n starting from \mathcal{M}_0 -which is analytically known from Eq. (2)-, keeping track of the noise realizations for $m = 0, 1, \dots, n-1$ and drawing the noise at the n -th step conditioned to the previous ones. This method does not require any convergence criterion for the global memory function, but only on the fluctuations of the new memory value being computed. However, the generation of the trajectories cannot be performed in Fourier space as explained above because of the bias introduced by the past realizations, and one needs to invert a correlation matrix at any time step. This method suffers, however, a serious limitation when applied to equilibrium dynamics. In fact, computing the matrix $\mathcal{M}_{m,n}$ using the TTI assumption as in Eq. (2), which gives $\mathcal{M}_{m,n} = \mathcal{M}_{0,|m-n|}$, preserves the positivity of $\mathcal{M}_{m,n}$ only in the limit of an infinite number of trajectories. With a finite number of trajectories, $\mathcal{M}_{m,n} = \mathcal{M}_{0,|m-n|}$ can have negative eigenvalues because of statistical fluctuations in the numerical solution. This issue would not be present if the memory function was computed without assuming TTI, because in that case it is easy to show that $\mathcal{M}_{m,n} \propto \langle \bar{v}'(h(m\Delta t)) \bar{v}'(h(n\Delta t)) \rangle$ (where the average is over trajectories with the proper initial conditions) is a positive-definite matrix for any number of simulated trajectories. However, calculating the memory in this way is more difficult, because it receives contributions from trajectories starting in any $h_0 > 0$, which introduces the non-trivial problem of finding an upper cutoff h_0^{\max} for the h_0 integral. Therefore, we only used this method to simulate short-time trajectories; the results we found agree with the fixed time grid method. Note that in future non-equilibrium studies [17, 20] the TTI hypothesis will have to be relaxed anyway, and this method is then more interesting than the fixed-grid method.

Another algorithm we considered is the so-called decimation algorithm [36]: because of the causality, one can compute \mathcal{M}_n on a fixed grid up to a final time t_1 with time steps Δt_1 ; then, one can double the time step and the final time, defining $\Delta t_2 = 2\Delta t_1$ and $t_2 = 2t_1$. The memory function is computed iteratively as on the fixed time grid, but keeping fixed the part of \mathcal{M}_n corresponding to $n\Delta t_2 < t_1$, using an exponential fit as initial condition on the second half, and so on, iteratively. This method has the great advantage of providing a higher resolution at short times, i.e. starting with a $\Delta t_1 \sim 10^{-5}$, and reaching final times $t_{\max} \sim 100$ with an increased efficiency with respect to the fixed time grid algorithm; however, at variance with the decimation algorithm used in numerical solutions of MCT-like equations [36], here we cannot increase Δt indefinitely because, while the memory function decays slowly at large times, the individual trajectories $h(t)$ still fluctuate wildly. Because we do not know the explicit time propagator of the probability density of h , the time step Δt must be kept small enough to ensure a correct integration of the equation of motion for $h(t)$. Furthermore, the main advantage of decimation algorithms is the speedup of the computation of the memory integral through the decomposition in a slow and a fast part [36]; unfortunately, this is not possible in our model because, once again, trajectories $h(t)$ cannot be split in a slow and fast decay, as it is usually done for correlation functions. Another minor problem of the decimation algorithm is the appearance of discontinuities in the solution for $\mathcal{M}(t)$ at the boundary of each grid, indicating an imperfect matching of numerical solutions when changing the time step Δt .

For all these reasons, most of the numerical results shown in section V are obtained via the fixed grid algorithm. In the specific case of Brownian Hard Spheres, however, we will show that because of the divergence of $\mathcal{M}(t)$ at short times, a decimation algorithm provides better solutions than the fixed grid algorithm.

C. Dynamical equation in discrete time

We now discuss how the DMFT equations (1) can be discretized over a fixed time grid with time steps Δt . We will use both the SSq potential and a HS potential, in the Brownian and Newtonian cases.

1. Soft Spheres

We obtained $N_T = N_H \times N_P$ trajectories determined by Eq. (1), integrating N_P independent noise realizations for each of N_H values of h_0 chosen on a uniform grid between h_{\min} and 0. Because the correlation of the noise $\Xi(t)$ has both a white and a colored contribution, we splitted it into two independent Gaussian noises $\Xi(t) = \xi(t) + \chi(t)$, having respectively $\langle \xi(t)\xi(u) \rangle = 2\delta(t-u)$ and $\langle \chi(t)\chi(u) \rangle = \mathcal{M}(t-u)$.

The Brownian dynamical Eq. (6), discretized within Itô calculus by the Euler-Maruyama method, reads

$$\begin{aligned} h_{n+1} &= h_n + (1 - \widehat{\varepsilon} h_n \theta(-h_n) - I_n + \chi_n) \Delta t + \sqrt{2\Delta t} \xi_n = h_n + \Delta h_n, \\ I_n &= \sum_{m=0}^{n-1} \mathcal{M}_{n-m} \Delta h_m. \end{aligned} \quad (54)$$

Here ξ_n and χ_n are independent random variables with zero average and correlations $\langle \xi_m \xi_n \rangle = \delta_{m,n}$ and $\langle \chi_m \chi_n \rangle = \mathcal{M}_{|m-n|}$. The memory kernel \mathcal{M}_n is updated after one iteration through the numerical evaluation of Eq. (53), namely

$$\mathcal{M}_n = \frac{\widehat{\varphi}}{2} \widehat{\varepsilon}^2 \sum_{i=1}^{N_H} e^{h_i - \widehat{\varepsilon} h_i^2/2} h_i \Delta h \frac{1}{N_P} \sum_{p=1}^{N_P} h_n^{(p,i)} \theta(-h_n^{(p,i)}), \quad (55)$$

where $\Delta h = |h_{\min}|/N_H$ and $h_i = h_{\min} + (i-1/2)\Delta h$, while $h_n^{(p,i)}$ is the p -th stochastic trajectory realized starting from h_i . The iterations are repeated until convergence, as explained in section IV B.

Within Newtonian dynamics, the second-order Eq. (8) can be written as a system of two coupled first-order equations for $h(t)$ and $g(t) = \dot{h}(t)$. The scheme is the same as for Brownian dynamics, except that one must draw an initial velocity g_0 from a normal distribution with unit variance, and we discretize the motion through a stochastic Verlet algorithm, which reads

$$\begin{aligned} f_n &= 1 - \widehat{\varepsilon} h_n \theta(-h_n) - I_n + \chi_n, \\ \widetilde{g}_n &= g_n + \frac{1}{2} f_n \Delta t, \\ h_{n+1} &= h_n + \widetilde{g}_n \Delta t, \\ g_{n+1} &= \widetilde{g}_n + \frac{1}{2} f_{n+1} \Delta t, \\ I_n &= \sum_{m=0}^{n-1} \mathcal{M}_{n-m} \Delta h_m, \end{aligned} \quad (56)$$

with $\langle \chi_m \chi_n \rangle = \mathcal{M}_{|m-n|}$. The numerical evaluation of \mathcal{M}_n is again obtained via Eq. (55), with an additional average over the random initial velocity, randomly drawn from a unit centered Gaussian.

2. Hard Spheres

In order to integrate the HS dynamics, one needs to implement an appropriate reflecting boundary condition at $h = 0$. Contrary to the SS case, all the trajectories that contribute to $\mathcal{M}(t)$ start from $h = 0$ and eventually collide with the boundary between t and $t + \Delta t$. Therefore one has $N_T = N_P$ because $N_H = 1$. Another problem is given by the interpretation of \mathcal{M}_0 , which is infinite for Hard Spheres, but that must be set equal to a physically meaningful value in the discretization.

For Brownian dynamics, we include the white component of the noise in the definition of the noise kernel. Therefore, we have $\langle \Xi_m \Xi_n \rangle = (2/\Delta t) \delta_{m,n} + \mathcal{M}_{|m-n|}$, we fix $\mathcal{M}_0 = 2/\Delta t$, and we only update the memory for $n > 0$. The infinite value of \mathcal{M}_0 and the short-time singularity $\mathcal{M}(t) \propto t^{-1/2}$ could in principle also affect the memory integral I_n ; however, when we approximate the retarded friction with a rectangle sum as in the last lines of Eqs. (54), (56), we then make

an error of order $\sqrt{\Delta t}$ in the integration, which becomes an error of order $\Delta t^{3/2}$ in the dynamical equation. For this reason, we neglect it as a first approximation. The Brownian dynamics is thus discretized with the rule

$$\begin{aligned} h_{n+1} &= |h_n + (1 - I_n + \Xi_n) \Delta t| = h_n + \Delta h_n, \\ I_n &= \sum_{m=0}^{n-1} \mathcal{M}_{n-m} \Delta h_m, \end{aligned} \quad (57)$$

where the modulus enforces the reflecting boundary condition in $h = 0$. A collision occurs between $n\Delta t$ and $(n+1)\Delta t$ if the argument of the modulus in Eq. (57) is negative; in this case, we add a count to the collisional probability at time n , which we call P_n . The latter quantity is related to the continuous-time return probability $p(0, t|0)$ defined in Eq. (25) observing that, for $\Delta t \ll 1$, a collision occur if $h_n + \sqrt{2\Delta t} \xi_n < 0$ (considering only the white part of the noise which dominates the short time motion). Therefore

$$\begin{aligned} P_n &\simeq \int_0^\infty dh p(h, t = n\Delta t|0) \int_{-\infty}^\infty \frac{d\xi}{\sqrt{2\pi}} e^{-\xi^2/2} \theta(-h - \sqrt{2\Delta t} \xi) \\ &= \int_0^\infty dh p(h, t|0) \Theta(-h/\sqrt{2\Delta t}) \simeq \sqrt{\frac{\Delta t}{\pi}} p(0, t|0), \end{aligned} \quad (58)$$

being $\Theta(x) = (2\pi)^{-1/2} \int_{-\infty}^x dz e^{-z^2/2}$ the normal cumulative distribution function and having also assumed that $p(h, t|0)$ is continuous for $h \rightarrow 0^+$. The numerical estimate of P_n is given by

$$P_n = \frac{1}{N_P} \sum_{p=1}^{N_P} C_n^{(p)} \quad (59)$$

being $C_n^{(p)} = 1$ if the p -th trajectory collides between $n\Delta t$ and $(n+1)\Delta t$, and 0 otherwise. Therefore, the memory kernel is computed at every iteration through the collisional probability P_n with the following expression, derived from Eq. (25):

$$\mathcal{M}_n = \frac{\hat{\varphi}}{2} \sqrt{\frac{\pi}{\Delta t}} P_n. \quad (60)$$

The algorithm for Newtonian Hard Spheres is similar. In this case, we only need to compute the regular part of the memory function as defined in Eq. (48), while we already know that there is a delta peak at $t = 0$ with amplitude $\zeta_0 = \sqrt{2/\pi} \hat{\varphi}$ as derived in section III B. We thus set $\mathcal{M}_0 = \zeta_0/\Delta t$ analogously to the Brownian case, and we simulate the dynamics with a single noise term Ξ_n having correlation $\langle \Xi_m \Xi_n \rangle = (\zeta_0/\Delta t) \delta_{m,n} + \mathcal{M}_{|m-n|}$. In this case, we discretize Eq. (49) with a stochastic Verlet algorithm, which reads

$$\begin{aligned} f_n(g_n) &= 1 - \zeta_0 g_n - I_n + \Xi_n, \\ \tilde{g}_n &= g_n + \frac{1}{2} f_n(g_n) \Delta t, \\ h_{n+1} &= |h_n + \tilde{g}_n \Delta t|, \\ g_{n+1} &= \begin{cases} \tilde{g}_n + \frac{1}{2} f_n(\tilde{g}_n) \Delta t & \text{if } h_n + \tilde{g}_n \Delta t > 0, \\ -g_n & \text{if } h_n + \tilde{g}_n \Delta t < 0, \end{cases} \\ I_n &= \sum_{m=0}^{n-1} \mathcal{M}_{n-m} \Delta h_m. \end{aligned} \quad (61)$$

Note that in case of a collision we simply reflect both the final position of the particle -as in the Brownian case- and the velocity, $g_{n+1} = -g_n$, i.e. in that case we do not use the Verlet construction. Because collisions happen at times that are separated by a $\mathcal{O}(1)$ interval, errors during collisions do not accumulate and it is safe to discard higher order corrections.

When a collision occurs, the collisional probability is updated as in the Brownian case; however, because in the Newtonian dynamics the memory function is given by Eq. (48), the collisions must be weighted. From Eq. (44), we know that the probability to collide between t and $t + \Delta t$ with velocity g_1 having started at $h = 0$ with velocity g_0 is equivalent to $f(g_1, t|g_0)$. Thus, from the third equivalence of Eq. (47) we need to measure the average of $2|g_1|C_n$,

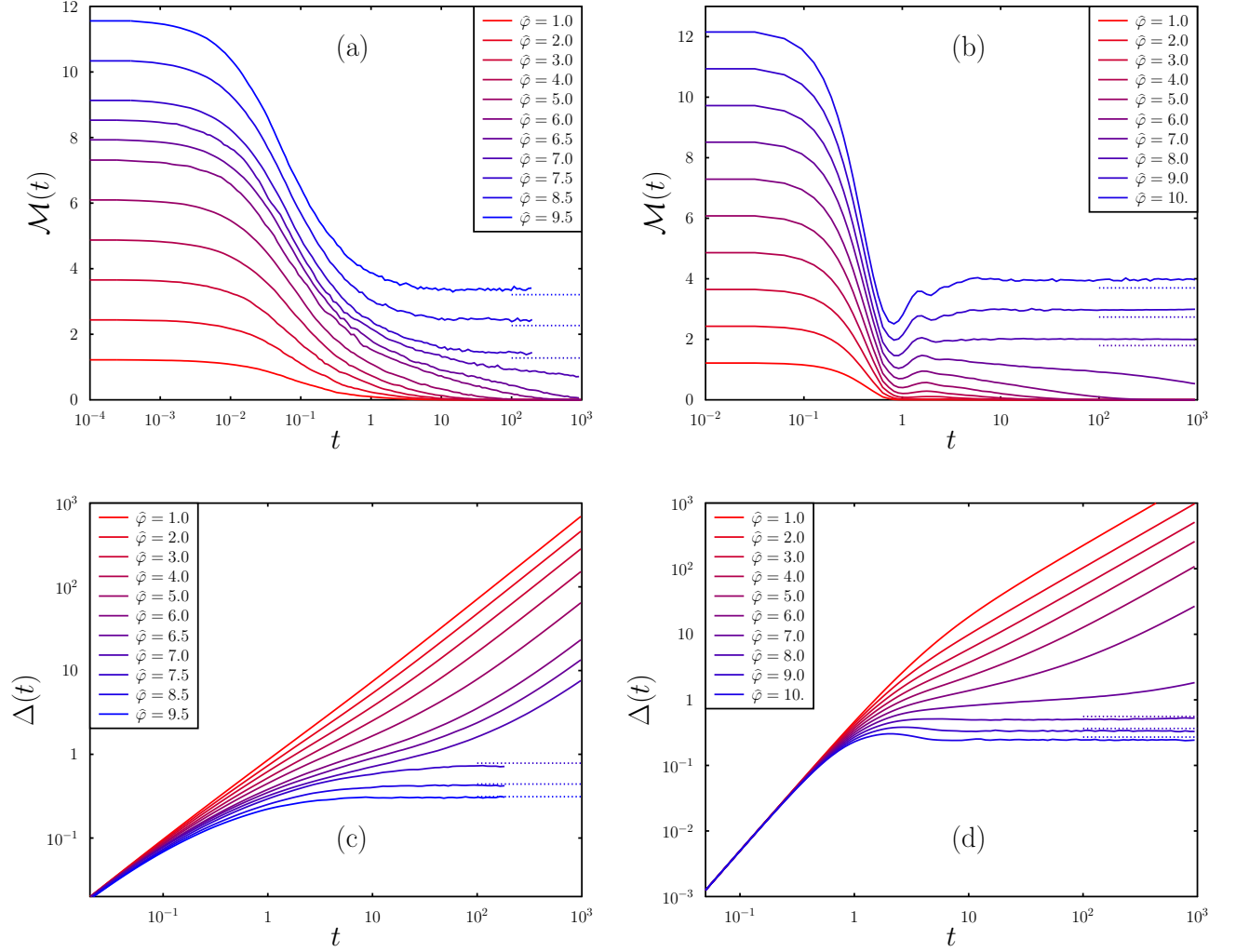


FIG. 1: Numerical solution of the DMFT equations for the quadratic Soft Sphere potential at $\hat{\varepsilon} = 10$ and several densities $\hat{\varphi}$. Top panels: memory kernels $\mathcal{M}(t)$ for Brownian (a) and Newtonian (b) dynamics. The memory functions in the liquid phase $\hat{\varphi} < \hat{\varphi}_d \simeq 7.2458$ decays over a time scale that increases upon approaching the dynamical transition. In the dynamically arrested phase $\hat{\varphi} > \hat{\varphi}_d$, a plateau emerges and $\mathcal{M}(t) \rightarrow \mathcal{M}_\infty > 0$ for long times. The value of $\mathcal{M}_\infty(\hat{\varphi})$ obtained from the plateau equation is plotted as a dashed lines with the same color of the corresponding density. Bottom panels: mean square displacement $\Delta(t)$ for Brownian (c) and Newtonian (d) dynamics. The long-time limit $\Delta_\infty = T^2/\mathcal{M}_\infty$ in the dynamically arrested phase is plotted as a dashed line.

being C_n the collisional event defined in the Brownian case and g_1 the precollisional velocity. The memory function is then given by

$$\mathcal{M}_n = \frac{\hat{\varphi}}{2} \frac{1}{N_P \Delta t} \sum_{p=1}^{N_P} 2 |g_{n-1}^{(p)}| C_n^{(p)}, \quad (62)$$

having started the trajectories in $h = 0$ with an initial velocity g_0 distributed as $P(g_0) = \sqrt{2/\pi} g_0^2 \exp(-g_0^2/2) \theta(g_0)$.

V. RESULTS

In this section, we present results for $\mathcal{M}(t)$ and $\Delta(t)$ for Soft and Hard Spheres, in both cases for Brownian and Newtonian dynamics. For Soft Spheres, we always use the quadratic potential, SSq with $\hat{\varepsilon} = 10$, unless otherwise

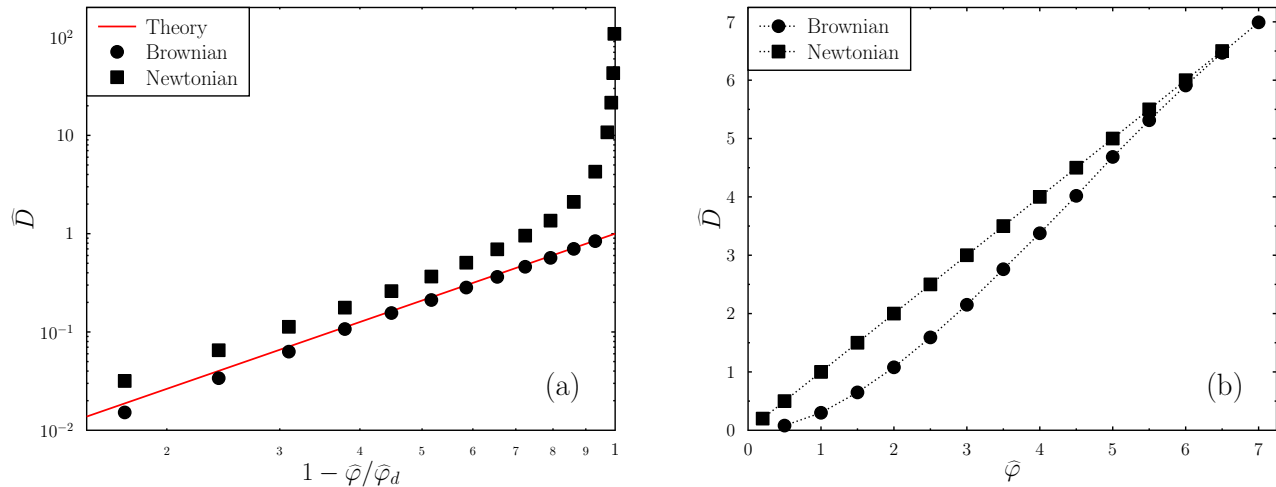


FIG. 2: Numerical solution of the DMFT equations for the quadratic Soft Sphere potential at $\hat{\varepsilon} = 10$ and several densities $\hat{\varphi}$. (a) Critical scaling of the diffusivity $\hat{D} \sim (\hat{\varphi}_d - \hat{\varphi})^\gamma$ for $\hat{\varphi} \rightarrow \hat{\varphi}_d^-$, for Brownian (circles) and Newtonian (squares) dynamics. The line is the analytical prediction with $\hat{\varphi}_d = 7.2458$ and $\gamma \simeq 2.25844$; the height of the line is adjusted to the plot. (b) Stokes-Einstein relation for Brownian and Newtonian dynamics, same key as left panel.

specified. From the analysis of the plateau equations derived in section IID, the dynamical glass transition happens at density $\hat{\varphi}_d \simeq 7.2458\dots$ in this case. For Hard Spheres, the dynamical glass transition is at $\hat{\varphi}_d = 4.8067\dots$

A. Soft Spheres

Results for $\mathcal{M}(t)$ obtained in Brownian and Newtonian dynamics are shown in Figs. 1a, 1b, respectively. The characteristic decay time of $\mathcal{M}(t)$ increases upon increasing density $\hat{\varphi}$, corresponding to a dynamical slowing down, which becomes heavily pronounced for $\hat{\varphi} = 7.0$. For $\hat{\varphi} \geq 7.50$, the memory exhibits a plateau as expected in the dynamically arrested phase. The numerical values of the memory can be compared to the analytical result for the plateau obtained from Eq. (13). The comparison is shown in Figs. 1a, 1b, with a fair agreement between analytical and numerical results.

From the knowledge of $\mathcal{M}(t)$, the mean square displacement (MSD) can be easily computed through Eq. (3): the numerical results for the MSD versus time are shown in Figs. 1c, 1d. For $\hat{\varphi} < \hat{\varphi}_d$, one finds the free particle behavior (diffusive for the Brownian and ballistic for the Newtonian dynamics) at short times and diffusive behavior at long times. Upon approaching the critical density $\hat{\varphi}_d$, the diffusion starts slowing down until the diffusion coefficient vanishes at $\hat{\varphi}_d$. A finite plateau, $\lim_{t \rightarrow \infty} \Delta(t) = \Delta_\infty$, is observed in the MSD at long times for $\hat{\varphi} > \hat{\varphi}_d$. The numerical long-time limit Δ_∞ can be compared to the theoretical one, which is given by $\Delta_\infty = T^2/\mathcal{M}_\infty$ from Eq. (3) [21].

We next discuss the critical behavior of the diffusivity upon approaching the dynamical transition. It is expected from the asymptotic analysis of the DMFT equations [21, 37] that the diffusion coefficient D defined in Eq. (4) follows a power-law behavior, i.e. $D \sim |\hat{\varphi}_d - \hat{\varphi}|^\gamma$ when $\hat{\varphi} \rightarrow \hat{\varphi}_d^-$, as in Mode Coupling Theory (MCT) [3]. The critical exponent γ can be computed for the SSq potential at $\hat{\varepsilon} = 10$, returning the value $\gamma \simeq 2.25844$ [21, 37]. The critical behavior is clearly seen in Fig. 2a. Interestingly, we find that in the Brownian case the power-law behavior is observed also for packing fractions rather distant from the critical point. On the other hand, the Newtonian diffusivity is diverging for low densities because of the ballistic motion in the absence of interactions. However, in both cases the agreement with the analytical results is very good; the difference in the prefactor is due to the difference in microscopic time units in Brownian and Newtonian dynamics.

In the $d \rightarrow \infty$ limit, the diffusion coefficient and the viscosity are related by a generalized Stokes-Einstein relation [15, 21, 38]. Indeed, the rescaled shear viscosity defined in Eq. (5) is given by the interaction term only when $d \rightarrow \infty$; therefore, Eqs. (4) and (5) lead to the Stokes-Einstein Relation (SER)

$$\beta \hat{D} \hat{\eta}_s = \frac{\beta \hat{\varphi} \int_0^\infty dt \mathcal{M}(t)}{\hat{\zeta} + \beta \int_0^\infty dt \mathcal{M}(t)} = \frac{\hat{\varphi}}{1 + \hat{\zeta} \hat{\varphi} / \hat{\eta}_s}, \quad (63)$$

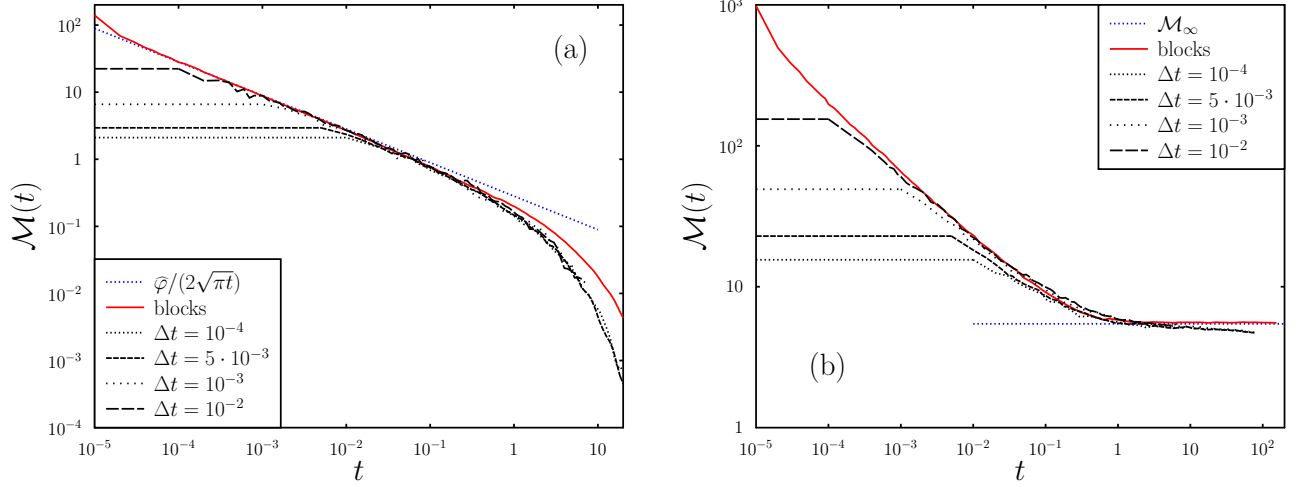


FIG. 3: Numerical solution of the DMFT for Brownian Hard Spheres. Comparison between $\mathcal{M}(t)$ obtained on a fixed grid (black lines) and with a decimation algorithm (continuous red line), at $\hat{\varphi} = 1.0$ (a) and 7.0 (b). The simulations with fixed time grid are plotted for several time steps Δt . The decimation algorithm has $\Delta t_{\min} = 10^{-5}$ and $\Delta t_{\max} = 2 \cdot 10^{-2}$. The dashed blue lines represent the short-time behaviour from Eq. (24) (left), and the analytical plateau \mathcal{M}_{∞} at $\hat{\varphi} = 7.0$ (right).

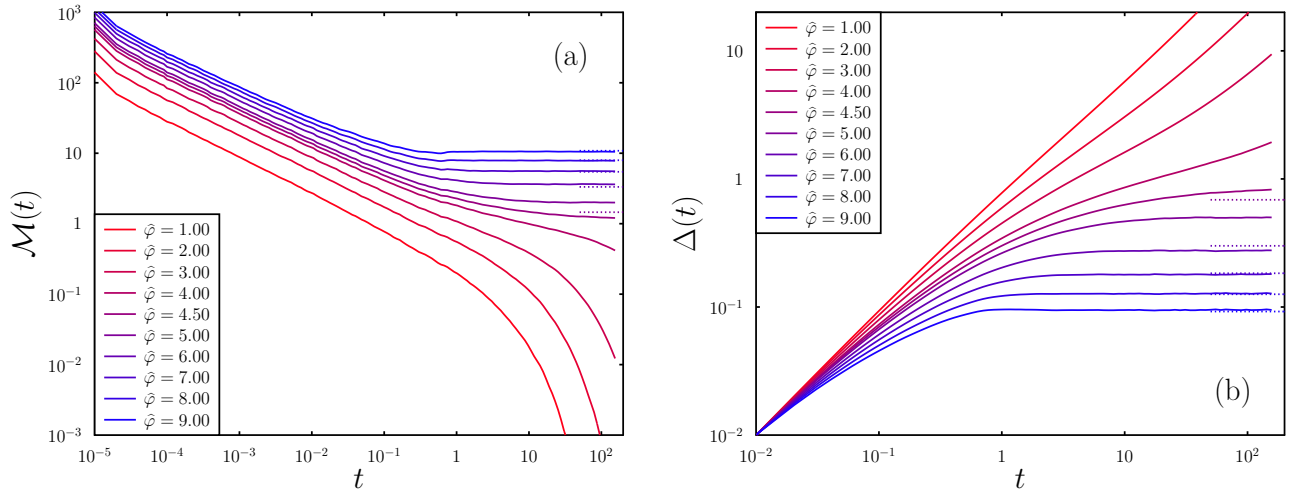


FIG. 4: Numerical solution of the DMFT for Brownian Hard Spheres obtained via the decimation algorithm. (a) Memory function $\mathcal{M}(t)$ for several packing fractions given in the legend. Dashed lines correspond to the analytical plateaus \mathcal{M}_{∞} when $\hat{\varphi} > \hat{\varphi}_d \simeq 4.8067$. (b) Mean square displacement $\Delta(t)$ computed from the corresponding $\mathcal{M}(t)$ figure, and comparison with the theoretical prediction of the plateau Δ_{∞} .

which is plotted as a function of $\hat{\varphi}$ in Fig. 2b. While this relation is trivial for the Newtonian case, in which $\beta \hat{D} \hat{\eta}_s = \hat{\varphi}$ because $\hat{\zeta} = 0$, the same is not true for Brownian dynamics, in which the linear behavior is only recovered asymptotically close to the dynamical transition, where the viscosity diverges.

B. Brownian Hard Spheres

The numerical results are less clear for Brownian Hard Spheres. In this case, we know from Eq. (24) that the short-time memory diverges as $t^{-1/2}$. We find that the numerical solution for $\mathcal{M}(t)$ depends on the discretization: in fact, the memory functions obtained through a fixed time grid and a decimation algorithm differ. The discrepancy is shown in Fig. 3, in which we show two cases with $\hat{\varphi} = 1.0$ and $\hat{\varphi} = 7.0$. Knowing that the critical density for

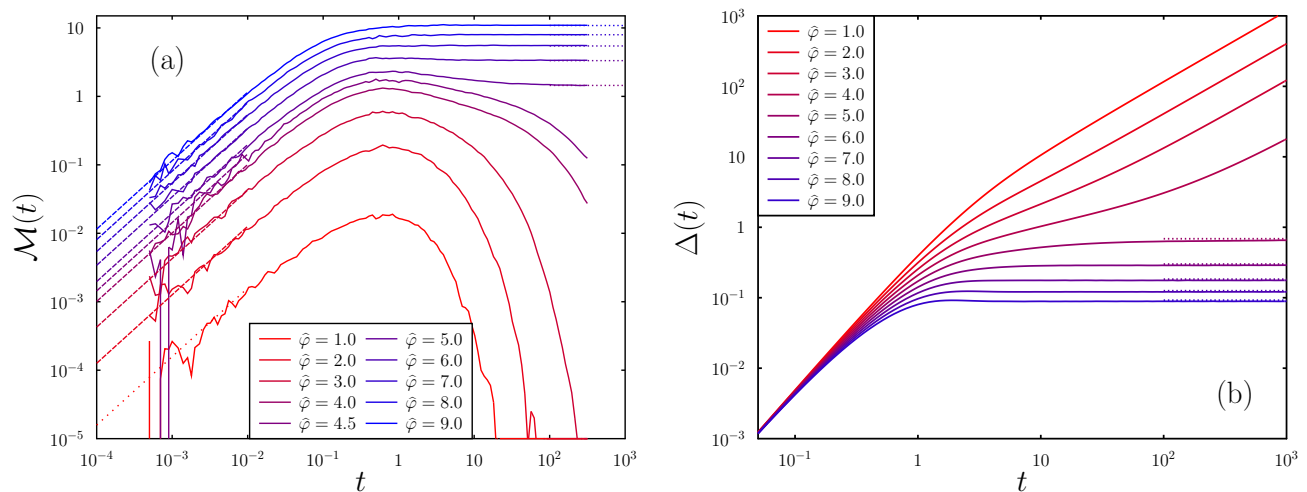


FIG. 5: Numerical solution of the DMFT equations for Newtonian Hard Spheres. (a) Memory kernel $\mathcal{M}(t)$. The numerical solution (continuous lines) is compared to the short-time prediction $\mathcal{M}(t) \sim Ct$ (dashed lines) and the expected plateau in the dynamically arrested phase (dotted lines). The curves are obtained by piecewise concatenation of the solution found with $\Delta t = 10^{-4}$ up to $t_{\max} = 1$ (short times) and the solution with $\Delta t = 5 \cdot 10^{-3}$ and $t_{\max} \sim 3 \cdot 10^2$. (b) Mean square displacement computed from the numerical $\mathcal{M}(t)$. The dotted lines correspond to the static plateau $\Delta_\infty = T^2/\mathcal{M}_\infty$.

Hard Spheres is $\hat{\varphi}_d \simeq 4.8067$, we expect to observe a complete decay in the dilute case and a plateau in the dense case. While the fixed-grid solution approaches the decimation solution for short times, there is a clear discrepancy at long times, which does not seem to depend on the time step Δt chosen for the fixed-grid algorithm. Moreover, the fixed-grid solution at $\hat{\varphi} = 7.0$ slowly decays below the plateau, while the decimation algorithm solution is going to the expected plateau $\mathcal{M}_\infty \simeq 5.45227$ obtained from Eq. (52). While we do not have a clear explanation for this discrepancy, we suspect that the short-time cutoff to the square root divergence imposed by the fixed time step affects the memory function even at long times. The decimation algorithm is able to partially cure this problem because the short-time part of the memory function is integrated more accurately. The results obtained with the decimation algorithm are thus closer to the theoretical predictions.

The memory function $\mathcal{M}(t)$ obtained via the decimation algorithm is shown in Fig. 3, for $\hat{\varphi} = 1.0, 2.0, \dots, 9.0$, and we observe a decay to zero in the liquid phase $\hat{\varphi} < \hat{\varphi}_d$ and a plateau in the solid phase $\hat{\varphi} > \hat{\varphi}_d$. However, the results display two main issues: first, there is a clear jump in the solution around $t \sim 1$ when we rescale $\Delta t \rightarrow 2\Delta t$, yielding an unphysical discontinuity in $\mathcal{M}(t)$. Second, the plateau is far from that obtained from Eq. (52) when $\hat{\varphi} \rightarrow \hat{\varphi}_d^+$. The reason for these discrepancies is unclear, and we unfortunately must conclude that our numerical integration schemes are not reliable for Brownian Hard Spheres.

C. Newtonian Hard Spheres

The fixed time grid algorithm works well when considering Newtonian Hard Spheres. Indeed, in this case the memory kernel can be separated into a singular and a regular part, see Eq. (37). The singular part provides a white noise contribution in the dynamics in Eq. (43) which can be discretized in a standard way, so we only need to compute self-consistently the regular part $\mathcal{M}_{\text{reg}}(t)$. We recall that a short-time exact analysis gives $\mathcal{M}_{\text{reg}}(t) \sim 0.1578 \hat{\varphi}^3 t$, see Appendix C 2. At long times, the memory function is expected to exhibit a plateau for $\hat{\varphi} > \hat{\varphi}_d \simeq 4.8067$. These asymptotic results are well reproduced by the numerical solution, as it can be seen in Fig. 5. The scaling of the diffusivity is shown in Fig. 5b. The diffusivity scaling $D \sim |\hat{\varphi}_d - \hat{\varphi}|^\gamma$ is confirmed, with the expected critical exponent $\gamma \simeq 2.33786$ [37].

In this paper we have not reported direct comparisons between the $d \rightarrow \infty$ results and numerical data in finite d because the latter are only available for $d \leq 10$ and finite d corrections are usually too large to prevent a direct comparison with the $d \rightarrow \infty$ solution, except for the critical scaling around the dynamical glass transition [32, 39]. However, an exception is given by the Stokes-Einstein relation for Newtonian dynamics, for which the finite d corrections seem unusually mild [32], which motivated us to attempt a systematic comparison with the solution of the DMFT equations. Note that in $d \rightarrow \infty$ the exact solution trivially gives $\beta \hat{D} \hat{\eta}_s = \hat{\varphi}$ for any potential. However,

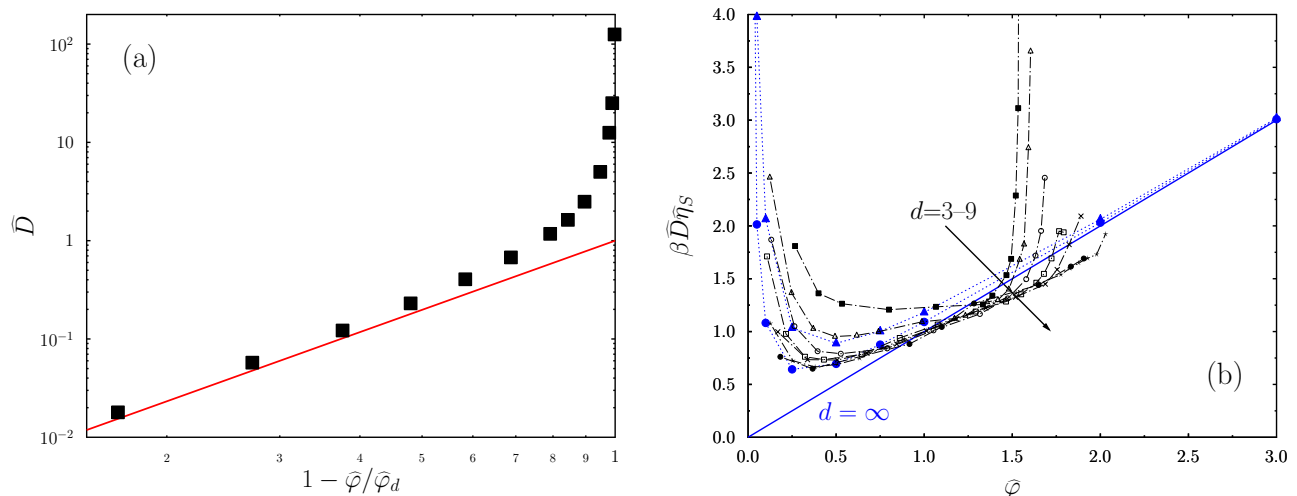


FIG. 6: Numerical solution of the DMFT equations for Newtonian Hard Spheres. (a) Critical scaling of the diffusivity $\hat{D} \sim (\hat{\varphi}_d - \hat{\varphi})^\gamma$ for $\hat{\varphi} \rightarrow \hat{\varphi}_d^-$, as in Fig. 2a but with $\hat{\varphi}_d = 4.8067$ and $\gamma = 2.33786$. (b) Stokes-Einstein relation including the kinetic viscosity for Newtonian Hard Spheres, numerically computed from Eq. (64) with $d = 8$ and $d = 12$ (blue points) and its $d = \infty$ limit (blue line). The black points correspond to MD simulations with $3 \leq d \leq 9$, from [32].

the kinetic term provides a $1/d$ correction that diverges in the dilute regime, leading to

$$\beta \hat{D} \hat{\eta}_s = \hat{\varphi} \left[1 + \frac{1}{d} \frac{\int_0^\infty du \ddot{\Delta}(u)^2}{\int_0^\infty du \mathcal{M}(u)} \right], \quad (64)$$

where the integrals are computed on the adimensional times $u = t/\tau_N$ and memory functions $\mathcal{M}(u) = \beta^2 \mathcal{M}(u \cdot \tau_N)$. The kinetic term vanishes in the $d \rightarrow \infty$ limit, but it also diverges in the dilute limit when $\hat{\varphi} \rightarrow 0$ because the motion becomes ballistic at all times and the integral of $\ddot{\Delta}(t)^2$ diverges (see Appendix C 3). In Fig. 6b we plot our results from Eq. (64) together with the finite-dimensional data. The divergence of $\beta \hat{D} \hat{\eta}_s$ at low $\hat{\varphi}$ in the Enskog regime is well visible, and the region over which it is observed shrinks upon increasing d , as expected. At finite value of $\hat{\varphi}$, the results from Eq. (64) thus converge to the line $\beta \hat{D} \hat{\eta}_s = \hat{\varphi}$ when $d \rightarrow \infty$. The finite- d numerical data agree well with Eq. (64) in the Enskog regime, while they seem to accumulate on a straight line with slope slightly smaller than one at higher density. We attribute this difference to the fact that d is not large enough. Note that the value of $\hat{\varphi}_d$ for $d = 8$ is around $\hat{\varphi}_d \sim 2$, hence still quite large from the asymptotic limit.

VI. CONCLUSIONS

In this work, we analyzed the DMFT equations for infinite-dimensional equilibrium liquids derived in [15–17]. We derived the DMFT equations for Hard Spheres as a limit of those for regular potentials, and we presented some methods to solve the DMFT equations numerically. Our numerical solution algorithm is based on a straightforward discretization of time and an iterative calculation of the kernel $\mathcal{M}(t)$ via the self-consistent condition.

For Soft Spheres (both Brownian and Newtonian) and Newtonian Hard Spheres, we obtain accurate numerical solutions which agree well with the expected asymptotic limits. The results confirm the presence of a dynamical glass transition with the same critical properties as Mode-Coupling Theory (although with different exponents), and provide the shape of the memory function and of the mean square displacement both in the liquid and glass phases. For Brownian Hard Spheres, the numerical integration scheme seem unable to properly handle the short time divergence of the memory function, and the resulting numerical solutions are not fully consistent with the asymptotic limit. Better discretization schemes should then be developed, which is a non-trivial problem in stochastic calculus.

This work opens the way to the numerical solution of the DMFT equations that describe non-equilibrium liquids [17, 20], which hopefully will give insight on a variety of phenomena such as yielding, jamming, and glass melting, both in passive and active systems.

Unfortunately, the algorithm is limited to relatively short times, as it is often the case in the study of DMFT equations, which prevents us to investigate long-time phenomena such as the dynamic criticality around the glass

transition (e.g. the stretching exponent of the memory function) and the aging dynamics in the glass phase [40].

Acknowledgments

We warmly thank P. Charbonneau, M. Fuchs and T. Franzosch for many useful exchanges, E. Agoritsas, J. Kurchan and T. Maimbourg for many discussions about the theoretical modeling, and G. Biroli and F. Roy for many insights about the numerical solution of the DMFT equations. This project has received funding from the European Research Council (ERC) under the European Union's Horizon 2020 research and innovation programme (grant agreement n. 723955 - GlassUniversality).

-
- [1] J.-P. Hansen and I. R. McDonald, *Theory of simple liquids (Third edition)* (Academic Press, 1986).
 - [2] U. Bengtzelius, W. Gotze, and A. Sjolander, *Journal of Physics C: Solid State Physics* **17**, 5915 (1984).
 - [3] W. Götze, *Complex dynamics of glass-forming liquids: a mode-coupling theory* (Oxford University Press, 2008).
 - [4] S. P. Das and G. F. Mazenko, *Physical Review A* **34**, 2265 (1986).
 - [5] A. Andreanov, G. Biroli, and A. Lefvre, *Journal of Statistical Mechanics: Theory and Experiment* **2006**, P07008 (2006).
 - [6] B. Kim and K. Kawasaki, *Journal of Physics A: Mathematical and Theoretical* **40**, F33 (2007).
 - [7] H. Jacquin and F. Van Wijland, *Physical Review Letters* **106**, 210602 (2011).
 - [8] W. Götze, *Journal of Physics: Condensed Matter* **11**, A1 (1999).
 - [9] H. L. Frisch, N. Rivier, and D. Wyler, *Physical Review Letters* **54**, 2061 (1985).
 - [10] H. Frisch and J. Percus, *Physical Review A* **35**, 4696 (1987).
 - [11] D. Wyler, N. Rivier, and H. L. Frisch, *Physical Review A* **36**, 2422 (1987).
 - [12] H. L. Frisch and J. K. Percus, *Physical Review E* **60**, 2942 (1999).
 - [13] T. R. Kirkpatrick and P. G. Wolynes, *Physical Review A* **35**, 3072 (1987).
 - [14] Y. Elskens and H. L. Frisch, *Physical Review A* **37**, 4351 (1988).
 - [15] T. Maimbourg, J. Kurchan, and F. Zamponi, *Physical Review Letters* **116**, 015902 (2016).
 - [16] G. Szamel, *Physical Review Letters* **119**, 155502 (2017).
 - [17] E. Agoritsas, T. Maimbourg, and F. Zamponi, *Journal of Physics A: Mathematical and Theoretical* **52**, 144002 (2019).
 - [18] A. Georges, G. Kotliar, W. Krauth, and M. J. Rozenberg, *Reviews of Modern Physics* **68**, 13 (1996).
 - [19] P. Charbonneau, J. Kurchan, G. Parisi, P. Urbani, and F. Zamponi, *Annual Review of Condensed Matter Physics* **8**, 265 (2017).
 - [20] E. Agoritsas, T. Maimbourg, and F. Zamponi, *Journal of Physics A: Mathematical and Theoretical* **52**, 334001 (2019).
 - [21] G. Parisi, P. Urbani, and F. Zamponi, *Theory of Simple Glasses: Exact Solutions in Infinite Dimensions* (Cambridge University Press, 2020).
 - [22] L. F. Cugliandolo, in *Slow relaxations and nonequilibrium dynamics in condensed matter*, edited by J. Barrat, M. Feigelman, J. Kurchan, and J. Dalibard (Springer-Verlag, 2003), [arXiv.org:cond-mat/0210312](https://arxiv.org/abs/cond-mat/0210312).
 - [23] A. J. Bray, S. N. Majumdar, and G. Schehr, *Advances in Physics* **62**, 225 (2013).
 - [24] R. A. Lionberger and W. B. Russel, *Journal of Rheology* **38**, 1885 (1994).
 - [25] R. Verberg, I. M. De Schepper, M. J. Feigenbaum, and E. G. D. Cohen, *Journal of Statistical Physics* **87**, 1037 (1997).
 - [26] E. Lange, J. B. Caballero, A. M. Puertas, and M. Fuchs, *The Journal of Chemical Physics* **130**, 174903 (2009).
 - [27] A. N. Borodin and P. Salminen, *Handbook of Brownian motion - facts and formulae* (Birkhäuser, 2012).
 - [28] J. W. Dufty, *Molecular Physics* **100**, 2331 (2002).
 - [29] A. Brańka and D. M. Heyes, *Physical Review E* **69**, 021202 (2004).
 - [30] I. M. De Schepper, M. H. Ernst, and E. G. D. Cohen, *Journal of Statistical Physics* **25**, 321 (1981).
 - [31] M. Bishop, J. Michels, and I. De Schepper, *Physics Letters A* **111**, 169 (1985).
 - [32] B. Charbonneau, P. Charbonneau, Y. Jin, G. Parisi, and F. Zamponi, *Journal of Chemical Physics* **139**, 164502 (2013).
 - [33] A. Singer and Z. Schuss, *Physical Review Letters* **95**, 110601 (2005).
 - [34] T. W. Burkhardt, *Journal of Statistical Mechanics: Theory and Experiment* **2007**, P07004 (2007).
 - [35] F. Roy, G. Biroli, G. Bunin, and C. Cammarota, *Journal of Physics A: Mathematical and Theoretical* **52**, 484001 (2019).
 - [36] B. Kim and A. Latz, *EPL (Europhysics Letters)* **53**, 660 (2001).
 - [37] J. Kurchan, G. Parisi, P. Urbani, and F. Zamponi, *The Journal of Physical Chemistry B* **117**, 12979 (2013).
 - [38] B. Charbonneau, P. Charbonneau, and G. Szamel, *The Journal of Chemical Physics* **148**, 224503 (2018).
 - [39] P. Charbonneau, E. I. Corwin, G. Parisi, and F. Zamponi, *Physical Review Letters* **109**, 205501 (2012).
 - [40] G. Folea, S. Franz, and F. Ricci-Tersenghi, [arXiv:1903.01421](https://arxiv.org/abs/1903.01421) (2019).
 - [41] M. Baity-Jesi and D. R. Reichman, *The Journal of Chemical Physics* **151**, 084503 (2019).
 - [42] J. A. Leegwater and H. van Beijeren, *Journal of Statistical Physics* **57**, 595 (1989).
 - [43] J. W. Dufty and M. H. Ernst, *Molecular Physics* **102**, 2123 (2004).
 - [44] T. W. Burkhardt, *Journal of Statistical Physics* **133**, 217 (2008).
 - [45] H. P. McKean, *Journal of mathematics of Kyoto University* **2**, 227 (1962).

Appendix A: Some details on Newtonian dynamics

We provide here some additional details on the formulation of the DMFT equations in the Newtonian case.

1. Distribution of the initial velocity

The distribution of the initial velocity \dot{h}_0 was not specified in [15, 17, 20] because it easily follows from the Maxwellian statistics of velocities in equilibrium. We provide some details here for completeness. Following [17, section 5.1], we define $y(t) = (\ell/d)\hat{\mathbf{r}}_0 \cdot (\mathbf{u}_1(t) - \mathbf{u}_2(t))$, where $\hat{\mathbf{r}}_0$ is the unit vector along the initial distance between two particles (essentially a random unit vector by isotropy), and $\mathbf{u}_{1,2}$ are the displacements of the two particles with respect to their initial position at time $t = 0$. According to the Maxwell distribution, each component of $\mathbf{u}_{1,2}$ is an independent Gaussian variable with zero mean and variance T/m . As a consequence, $\dot{y}(t)$ is also a random Gaussian variable with zero mean and variance $(d^2/\ell^2)2T/m = T/\hat{m}$. Finally, $h(t) = h_0 + y(t) + \Delta(t)$ and $\Delta(t)$ is ballistic at short times, hence $\dot{\Delta}(0) = 0$, which implies that $\dot{h}_0 = \dot{h}(0) = \dot{y}(0)$ is also a Gaussian variable with zero mean and standard deviation T/\hat{m} . This justifies the probability distribution of \dot{h}_0 in Eq. (2).

2. Viscosity

The derivation of the viscosity in $d \rightarrow \infty$ is discussed in [15, 21] where, however, the kinetic term has been omitted. We provide here a more detailed discussion that is needed to compare with simulation results.

The shear viscosity is given in terms of the autocorrelation of the stress tensor in [1, Eq.(8.4.10)]. The stress tensor, as given in [1, Eq.(8.4.14)], is the sum of a kinetic and an interaction terms. The contribution of the autocorrelation of the interaction term has been discussed in [21, section 3.8.1], and is given by $\eta_s = \beta\rho d \int_0^\infty dt \mathcal{M}(t)$. The other terms are subdominant when $d \rightarrow \infty$, but the autocorrelation of the kinetic term provides a divergent contribution for $\hat{\varphi} \rightarrow 0$ that we need to add if we want to properly reproduce the ideal gas limit.

We are then going to neglect the cross-correlation of the kinetic and interaction terms, because it is subdominant both in $1/d \rightarrow 0$ and in $\hat{\varphi} \rightarrow 0$, as deduced from [1, Eq.(8.4.21)] and [32, Eq.(D2)]. The autocorrelation of the kinetic term can be written, neglecting velocity correlation between distinct particles in the limit $\hat{\varphi} \rightarrow 0$, as

$$\eta_K = \beta\rho m^2 \int_0^\infty dt Z(t)^2, \quad Z(t) = \langle v_\mu(t)v_\mu(0) \rangle = \frac{1}{2d} \frac{d^2}{dt^2} \langle |\mathbf{r}(t) - \mathbf{r}(0)|^2 \rangle, \quad (\text{A1})$$

where $Z(t)$ is the autocorrelation of a single spatial component of the velocity [1, Eq.(7.2.1)], related to the mean square displacement by [1, Eq.(7.2.5)] (here we considered a representative particle, without indicating explicitly the average over the N particles). Recalling the scaling of mass and mean square displacement defined in section II A, we obtain

$$\eta_K = \beta\rho\hat{m}^2 \int_0^\infty dt \ddot{\Delta}(t)^2. \quad (\text{A2})$$

Summing the kinetic and interaction contributions, we obtain Eq. (5).

Appendix B: Brownian Hard Spheres

1. Derivation of the Laplace transform of the first iteration

We provide here some details on the solution of Eq. (18) with boundary conditions in Eq. (19). Consider the Laplace transform $\tilde{G}(h_0, s) = \int_0^\infty dt e^{-st} G(h_0, t)$. Using an integration by parts,

$$\int_0^\infty dt e^{-st} \dot{G}(h_0, t) = s\tilde{G}(h_0, s) + [e^{-st}G(h_0, t)]_0^\infty = s\tilde{G}(h_0, s) - G(h_0, 0), \quad (\text{B1})$$

and taking into account the first boundary condition in Eq. (19), we get

$$\begin{aligned} s\tilde{G}(h_0, s) - 1 &= \tilde{G}''(h_0, s) + (1 + \hat{\varepsilon})\tilde{G}'(h_0, s), & h_0 < 0, \\ s\tilde{G}(h_0, s) &= \tilde{G}''(h_0, s) + \tilde{G}'(h_0, s), & h_0 > 0. \end{aligned} \quad (\text{B2})$$

Taking into account the two other boundary conditions in Eq. (19), the solution is given by Eq. (20) with yet unknown functions $c_{\pm}(s)$. Now we should impose the continuity conditions in $h_0 = 0$. The leading singularity in Eq. (B2) is of the form $\tilde{G}'''(h_0, s) \approx \theta(h_0)$ (note that a jump singularity comes from both the right and left hand sides of the equation), which implies that $\tilde{G}(h_0, s)$ and $\tilde{G}'(h_0, s)$ are both continuous functions of h_0 . This gives the conditions

$$\begin{aligned} \frac{1}{s} + c_-(s) &= c_+(s) , \\ c_-(s)\lambda_-(s) &= c_+(s)\lambda_+(s) , \end{aligned} \quad (\text{B3})$$

which imply

$$c_-(s) = \frac{\lambda_+(s)}{s[\lambda_-(s) - \lambda_+(s)]} , \quad c_+(s) = \frac{\lambda_-(s)}{s[\lambda_-(s) - \lambda_+(s)]} , \quad (\text{B4})$$

thus completing the proof of Eq. (20).

2. Short-time behavior of the stress-stress correlation

The short-time behavior of the stress autocorrelation function $C_{\sigma\sigma}(t) = \beta \langle \Pi_{\mu\nu}(t)\Pi_{\mu\nu}(0) \rangle / V$ [1, 21] for Brownian Hard Spheres is given by kinetic theory for $d = 3$ [24–26], as

$$C_{\sigma\sigma}(t \rightarrow 0) = \frac{18}{5} \varphi^2 g(\ell) \frac{\eta_0}{\tau} \sqrt{\frac{2\tau}{\pi t}} = \frac{24}{5\pi} \varphi^2 g(\ell) \frac{T}{\ell^3} \sqrt{\frac{2\tau}{\pi t}} , \quad (\text{B5})$$

where ℓ is the sphere diameter, φ is the packing fraction, $g(\ell)$ is the contact value of the pair correlation function, $D_0 = T/\zeta$ is the free particle diffusion coefficient, $\tau = \ell^2/(4D_0)$, and η_0 is given by the Stokes expression $D_0 = T/(3\pi\eta_0\ell)$.

According to [15, 21], when $d \rightarrow \infty$, the stress-stress autocorrelation is simply related to the memory function by

$$C_{\sigma\sigma}(t) = \beta \rho d \mathcal{M}(t) , \quad \mathcal{M}(t \rightarrow 0) \sim \frac{\hat{\varphi}}{2} T^2 \sqrt{\frac{\tau_B}{\pi t}} \quad \Rightarrow \quad C_{\sigma\sigma}(t \rightarrow 0) \sim \frac{2^{2d}\Gamma(1+d/2)}{2d\pi^{d/2}} \varphi^2 \frac{T}{\ell^d} \sqrt{\frac{2\tau}{\pi t}} , \quad (\text{B6})$$

where we used the short-time result for Brownian Hard Spheres reintroducing physical dimensions, with $\tau_B = \hat{\zeta}/T = (\ell^2/2d^2)\zeta/T = (\ell^2/2d^2)/D_0 = 2\tau/d^2$, and $\rho = 2^d \varphi / (V_d \ell^d)$ with $V_d = \pi^{d/2}/\Gamma(1+d/2)$.

The two expressions in Eq. (B5) and (B6) match if we recall that $g(\ell) \rightarrow 1$ when $d \rightarrow \infty$ [21], and if we interpret the factor 5 as $d+2$ in Eq. (B5). This leads us to conjecture that in generic dimension d ,

$$C_{\sigma\sigma}(t \rightarrow 0) \sim \frac{2^{2d}\Gamma(1+d/2)}{2(d+2)\pi^{d/2}} \varphi^2 g(\ell) \frac{T}{\ell^d} \sqrt{\frac{2\tau}{\pi t}} , \quad (\text{B7})$$

which coincides with Eq. (B5) in $d = 3$ and with Eq. (B6) when $d \rightarrow \infty$, hence $d+2 \approx d$.

Appendix C: Newtonian Hard Spheres

1. Short-time expansion from kinetic theory

In infinite dimensions, the memory function is related to the velocity autocorrelation [41]. We follow the notations of [21] and denote the non-scaled mean square displacement by $D(t) = \langle |\mathbf{r}(t) - \mathbf{r}(0)|^2 \rangle$. According to Eq. (A1), the velocity autocorrelation is $Z(t) = \dot{D}(t)/(2d)$ [1]. In the infinite dimensional limit, for Newtonian dynamics, the non-scaled memory function $M(t) = (2d^2/\ell^2)\mathcal{M}(t)$ is related to $D(t)$ by [21]

$$m\ddot{D}(t) = 2dT - \beta \int_0^t du M(t-u) \dot{D}(u) , \quad (\text{C1})$$

which in Laplace space, using $s^2\tilde{D}(s) = 2d\tilde{Z}(s)$, reads

$$m\tilde{Z}(s) = T/s - \beta\tilde{M}(s)\tilde{Z}(s)/s \quad \Rightarrow \quad \tilde{M}(s) = \frac{T - ms\tilde{Z}(s)}{\beta\tilde{Z}(s)} . \quad (\text{C2})$$

Kinetic theory [30, 31, 42, 43] gives the short-time expansion of $Z(t)$ in arbitrary dimension as

$$\frac{Z(t)}{Z(0)} = 1 - \frac{2|t|}{d\tau_E} + A_d \left(\frac{t}{\tau_E} \right)^2 + \mathcal{O}(t^3), \quad \tau_E = \frac{\sqrt{\pi\beta m}}{d2^d\varphi} \frac{\ell}{g(\ell)}, \quad A_d = \frac{2}{d^2} {}_2F_1 \left(-\frac{1}{2}, -\frac{1}{2}; \frac{1}{2}(d+2); \frac{1}{4} \right), \quad (\text{C3})$$

where $Z(0) = T/m$. Moving to Laplace space and plugging this expansion in Eq. (C2) we get

$$\widetilde{M}(s) = \frac{2Tm}{d\tau_E} \left[1 + \frac{2(1-A_d)}{d\tau_E} \frac{1}{s} + \mathcal{O}\left(\frac{1}{s^2}\right) \right]. \quad (\text{C4})$$

This result shows that $M(t)$ is indeed the sum of a delta function and a regular function, which admits a short time expansion in integer powers of t . Taking the $d \rightarrow \infty$ limit with the rescaling $\widehat{m} = (\ell^2/2d^2)m$, $2^d\varphi = d\widehat{\varphi}$, $\mathcal{M}(t) = (\ell^2/2d^2)M(t)$, and using $g(\ell) \rightarrow 1$ and $A_d = 1 + \alpha/d + \dots$, we obtain

$$\widetilde{\mathcal{M}}(s) = \widehat{\varphi} \sqrt{\frac{2T\widehat{m}}{\pi}} \left[1 - \frac{2\alpha}{d\tau} \frac{1}{s} + \mathcal{O}\left(\frac{1}{s^2}\right) \right], \quad \tau = d\tau_E = \frac{\sqrt{2\pi\beta\widehat{m}}}{\widehat{\varphi}}. \quad (\text{C5})$$

This result proves Eq. (36) when transformed back to the time domain. In particular, the coefficient of the delta peak coincides with the result obtained from DMFT, and the value of $\mathcal{M}_{\text{reg}}(t=0)$ is found to vanish proportionally to $1/d$ for $d \rightarrow \infty$. Unfortunately, to our knowledge the next term of the short-time expansion has not been computed.

2. Short-time expansion of the regular part of the memory function within DMFT

The regular part of the memory function $\mathcal{M}_{\text{reg}}(t)$ for Newtonian Hard Spheres can be analytically computed for short times. Keeping only the leading short-time singularity $\mathcal{M}(t) = 2\zeta_0\delta(t)$ as given in Eq. (34), the evolution of $h(t)$ reads

$$\begin{aligned} \ddot{h}(t) + \zeta_0\dot{h}(t) &= 1 + \Xi(t), \quad h(t) > 0 \\ h(t=0) &= 0, \quad \dot{h}(t=0) = g_0, \\ \langle \Xi(t)\Xi(u) \rangle &= 2\zeta_0\delta(t-u). \end{aligned} \quad (\text{C6})$$

Because this white noise dominates at short times, we expect that in order to obtain the short-time behavior of $\mathcal{M}_{\text{reg}}(t)$ we can neglect the regular part in the stochastic process, i.e. we use the process in Eq. (C6). Furthermore, at short times we can approximate the return probability by the *first* return probability, i.e. neglect multiple returns. The computation of the first return density probability $f(g_1, t|g_0)$ defined in Eq. (45) is a Wang-Uhlenbeck recurrence time problem. Note that in the absence of the term $\zeta_0\dot{h}(t)$, Eq. (C6) reduces to the random acceleration process in the presence of a linear drift [34], for which the first passage time distribution can be computed exactly [44]. In presence of the linear drift, the problem can be solved analytically for short times. In our units, we obtain [33] (see also [44, 45])

$$f(g_1, t|g_0) \sim \frac{\sqrt{3}|g_1|}{2\pi\zeta_0 t^2} \exp\left(\frac{g_0^2 - g_1^2}{4} - \frac{g_0 - g_1}{2\zeta_0} - \frac{g_1^2 + g_1g_0 + g_0^2}{\zeta_0 t}\right) \text{erf}\left(\sqrt{\frac{3|g_1|g_0}{\zeta_0 t}}\right). \quad (\text{C7})$$

The latter result can be plugged into Eq. (48), and the integral can be performed with the change of variables $u_i = |g_i|/\sqrt{\zeta_0 t}$ for $i = 0, 1$ and expanding around $t = 0$. Setting now $\zeta_0 = \sqrt{2/\pi}\widehat{\varphi}$, one finds

$$\mathcal{M}_{\text{reg}}(t) \sim \frac{\sqrt{6}}{\pi^{5/2}} \left[\int_0^\infty du_0 \int_0^\infty du_1 u_0^2 u_1^2 e^{-(u_1^2 - u_0 u_1 + u_0^2)} \text{erf}\left(\sqrt{3u_1 u_0}\right) \right] \widehat{\varphi}^3 t = C_0 \widehat{\varphi}^3 t, \quad (\text{C8})$$

with $C_0 \simeq 0.1578$. This result confirms that $B = 0$ and $C = C_0 \widehat{\varphi}^3$ when $d = \infty$ in Eq. (36). This short-time behavior has been plotted in Fig. 5a, showing a good agreement between theory and simulations, especially at high densities.

3. Low-density regime of the DMFT equations

When $\widehat{\varphi} \ll 1$, the regular part of the memory function is negligible, therefore $\mathcal{M}(t) = 2\zeta_0 \delta(t)$. Using Eq. (3) in adimensional units, with the above-mentioned memory kernel and $\widehat{\zeta} = 0$ one finds the solution

$$\Delta(t) = \frac{1}{\zeta_0} \left[t - \frac{1}{\zeta_0} \left(1 - e^{-\zeta_0 t} \right) \right], \quad (\text{C9})$$

corresponding to the characteristic MSD of underdamped, dilute dynamics, with a ballistic regime for $t \ll \zeta_0^{-1}$ and a diffusive regime for $t \gg \zeta_0^{-1}$. This allows one to compute analytically the viscosity and diffusion constant. The two integrals in Eq. (64) can be explicitly computed and give $\int_0^\infty du \dot{\Delta}(u)^2 = (2\zeta_0)^{-1}$ and $\int_0^\infty du \mathcal{M}(u) = \zeta_0$. Recalling that $\zeta_0 = \sqrt{2/\pi} \widehat{\varphi}$, one finds

$$\beta \widehat{D} \widehat{\eta}_s = \widehat{\varphi} \left(1 + \frac{\pi}{4d \widehat{\varphi}^2} \right), \quad (\text{C10})$$

leading to the dilute-limit divergence $\beta \widehat{D} \widehat{\eta}_s \approx \pi/(4d \widehat{\varphi})$ when $\widehat{\varphi} \rightarrow 0$ in any finite dimension. This divergence disappears when $d \rightarrow \infty$.